Use of Nano-Metal Particles for Promoting Aquathermolysis Reaction during Cyclic Steam Stimulation

By

Siyuan Yi

A Thesis Submitted in Partial Fulfillment of the Requirements for the Degree of

Master of Science

in

Petroleum Engineering

Department of Civil and Environmental Engineering

University of Alberta

ABSTRACT

Cyclic steam stimulation (CSS) is one of the commonly used thermal extraction methods for heavy oil and bitumen. However, CSS is still daunted by the lower oil recovery factor compared with other thermal recovery methods, such as steam-assisted gravity drainage (SAGD). Nano-metal particles, due to a high surface to volume ratio, can catalyze the reactions and *in-situ* upgrade heavy oil, which could potentially help to increase the oil recovery factor in CSS.

This thesis aims to investigate the catalytic effect of different types of nano-metal particles on oil recovery factor. A series of recovery experiments simulating the CSS process were first conducted using nickel nanoparticles. The optimum nickel nanoparticle concentration, the effect of the particle's penetration depth on oil recovery, and the performance of the particles at lower temperatures were investigated in detail. Experimental results show that the best concentration of nickel nanoparticle, which gave the highest ultimate oil recovery factor (RF), was 0.20 wt% of initial oil in place (IOIP) under 220°C, whereas the nickel concentration of 0.05 wt% provided the highest RFs at the early stages. A lower temperature of 150°C provided a much-lower RF than 220°C, which was mainly because of a lower level of aquathermolysis reactions. By analyzing the compositions of produced oil and gas samples with saturates-asphaltenes-resins-aromatics (SARA) test and gas-chromatography (GC) analysis, we confirm that the major reaction mechanism during the aquathermolysis reaction is the breakage of the carbon/sulfur (C/S) bond; the nickel nanoparticles can act as catalyst for the aquathermolysis reaction; and the catalytic effect becomes less remarkable from cycle to cycle. One run of the experiment to test the effect of particle-penetration depth revealed that the nickel nanoparticles distributed near the injection port greatly contributed to the ultimate RF.

Next, a series of CSS experiments with the use of nickel and iron oxide nanoparticles were conducted under 220°C to compare their performance in promoting the aquathermolysis. During the experiments, we monitored the variations of oil recovery factor, produced-oil viscosity, produced-gas composition, and water production. The experimental results show that both nickel and iron oxide nanoparticles can act as catalyst for aquathermolysis reactions and reduce the viscosity of heavy oil. However, their catalytic effect differs dramatically. Nickel nanoparticle can break C-S bond more effectively than iron oxide nanoparticle, together achieving a higher ultimate oil recovery factor. Along with the boosted oil production, the water production was also increased from the very first cycle after introducing the nano-metal particles in CSS. The GC analysis and the pressure data recorded during each soaking period revealed that a higher amount of evolved gas was generated in the early stage, which increased the reservoir pressure and forced more condensed water produced from the sandpack.

The last part of this thesis mainly focuses on how to achieve stabilized nickel nanoparticle suspensions. To stabilize the nickel nanoparticle suspension, Xanthan gum polymer and surfactant (SDS, CTAB or Hypermer KD-2) were introduced into the nickel nanoparticle suspensions. Visual tests were then conducted to observe how the nickel nanoparticles would settle in the suspensions; factors, including polymer concentration, surfactant type, surfactant concentration, were considered in the tests. Zeta potentials of the suspensions were also measured. The following three nickel nanoparticle suspensions recipes were found to be most stable:

1. 1 wt% Ni/0.35 wt% SDS/0.045 wt% Xanthan;
2. 1 wt% Ni/0.35 wt%/Hypermer KD-2/0.045 wt% Xanthan; and
3. 2 wt% Ni/0.5 wt% SDS/0.06 wt% Xanthan.

Micromodel-based visualization tests were conducted on the three suspensions to reveal how the nickel nanoparticles would travel and distribute in the porous media when being injected into the porous media. Test results showed that most nickel nanoparticles were able to pass through the gaps between the sand grains; only a small amount of the nickel nanoparticles became attached to the grain surface. A higher nickel concentration in the suspension could lead to agglomeration of nickel nanoparticles in the porous media, while a lower concentration could mitigate this problem. Moreover, clusters tended to form when the nickel nanoparticle suspension carried an electrical charge opposite to that of the porous media. Follow-up water flooding was initiated after the nanofluid injection. It was found that the water flooding could not flush away the nanoparticles remaining in the micromodel.

ACKNOWLEDGMENTS

First of all, I would like to express my deepest gratitude to my parents Mr. Jun Yi and Mrs. Yunsu Zhao for their endless love, support and encouragement.

I am grateful for my supervisors Dr. Huazhou Andy Li and Dr. Tayfun Babadagli who provided me with the valuable opportunity to study at the University of Alberta. They gave constructive advice and guidance throughout my two-year study. I am thankful for all the time and patience they devoted to this work.

This research was conducted under Prof. Tayfun Babadagli's NSERC Industrial Research Chair in Unconventional Oil Recovery (industrial partners are Petroleum Development Oman, Total E&P Recherche Développement, SIGNa Oilfield Canada, CNRL, SUNCOR, Touchstone Exploration, Sherritt Oil, PEMEX, Husky Energy, Saudi Aramco, Devon. and APEX Eng.) and NSERC Discovery Grant (No: RES0011227 and NSERC RGPIN 05394) to Dr. Tayfun Babadagli and Dr. Huazhou Andy Li, respectively. I gratefully acknowledge these supports.

I would like to thank Dr. Babadagli's lab technicians Mr. Lixing Lin, Ms. Georgeta Istratescu, and Mr. Todd Kinnee for their endless assistance in the lab experiments, and Ms. Pam Keegan for editing all the papers and thesis. I am also thankful for all the EOGRRC group members and all my colleagues in Dr. Huazhou Andy Li's research group.

Finally, I would like to thank my boyfriend Mr. Yujie Su for his support through my tough times, and all my friends in Edmonton, especially Yujia Guo, Ruixue Li, Wanying Pang, and You Wei, for their friendship. I feel so lucky to have these friends far away from home.

TABLE OF CONTENTS

LIST OF TABLES

LIST OF FIGURES

CHAPTER 1 Introduction

1.1. Research Background

With the rapid advances of exploration and production techniques, heavy oil and bitumen start to play an increasingly important role in the world petroleum industry. Traditional heavy oil was described as oil (or gas-free oil) with API gravity below 21°API and viscosity between 100 and 10,000 centipoise (cP) at reservoir conditions (Banerjee 2012). However, Canadian heavy oil, mainly contained in oil sands or carbonates, normally has an API gravity less than 10° and viscosity above 10,000 cP at reservoir conditions. Due to its high viscosity, Canadian heavy oil can sometimes appear to be in solid state under room temperature, i.e., so-called bitumen (Banerjee 2012).

Alberta's oil sands reserve is considered to be one of the largest in the world, containing 1.8 trillion barrels of bitumen initially in-place (Government of Alberta 2012). However, production of heavy oil via natural drive mechanisms is not efficient due to its high viscosity (Prats 1978). Thermal methods can be very effective in reducing heavy oil viscosity, leading to enhanced oil recovery. Several thermal recovery methods are now widely used in the industry, including in-situ combustion (ISC), steam-assisted gravity drainage (SAGD), and cyclic steam stimulation (CSS).

CSS, also known as huff-and-puff, is one of the very first steam injection technologies developed in the early 1960s; its typical field applications include the Cold Lake oil sands in Canada and Liaohe oilfield in China. This method is effective in recovering heavy oil, especially in the first few cycles. However, ultimate recovery by CSS is lower (10-40% of original oil in place (OOIP)), compared to that of steam flooding and SAGD with over 50% of OOIP (Alvarez and Han 2013). Thus, many techniques have been recently proposed to further enhance the performance of CSS. One of these techniques is to use nano-metal particles to help catalyze the aquathermolysis reactions between water and heavy oil.

According to Clark and Hyne (1983), when heavy oil is being treated with steam, the viscosity reduction is not only a result of high temperature, but also related to a series of chemical reactions called aquathermolysis. During this process, the chemical bonds in large molecules, especially carbon-sulfur bond, can be cleaved, forming smaller molecules and releasing gases such as H_2S, CO_2 and H_2. Transition metal species are proved to catalyze the aquathermolysis

reactions and reduce the oil viscosity. Thus, more detailed research is needed to find a proper metal species which is able to boost the oil production in a cost-effective manner.

1.2. Statement of Problem

In CSS, the viscosity of heavy oil can be decreased dramatically during the production period. However, the viscosity of recovered oil tends to increase along with the drop of temperature and may even exceed the original viscosity of the because of the distillation caused by steam. Clark (1990) first reported that a viscosity reduction of heavy oil can be achieved by introducing a series of transition metal ionic solution. Several metal species were tested for seven oil types and the viscosity reduction was found for all the seven different heavy oils. Later on, Fan et al. (2002) proved the catalytic effect of metal species. Afterwards, Hamedi-Shokrlu and Babadagli (2014ab) conducted a series of detailed investigation on the catalytic effect of nickel nanoparticles. They clarified the kinetics of the aquathermolysis reactions as well as the effect of particle size (micron-sized and nano-sized) on promoting aquathermolysis reactions. However, in their study, the whole experimental setup used in the CSS experiments was placed inside an oven, implying almost zero heat loss from the system to the surroundings. Thus, although very promising and valuable data were obtained in their work, such setup is not representative of CSS production from a real reservoir. More representative experiments, to simulate the real CSS process need to be conducted. Meanwhile, nickel is an expensive catalyst, and also a poisonous metal that may cause health problems. Therefore, the catalytic effect of other metals should be explored in order to find a cheaper and safer alternative.

To better simulate the field condition, the nickel nanoparticle should be introduced into the reservoir in the form of nanofluid that is stable under reservoir conditions. However, nanoparticles have a high tendency of agglomeration due to high surface energy, making their suspension in a base fluid challenging (Li et al. 2007). Therefore, to achieve a better recovery performance, it is of critical importance to ensure that the nanoparticle suspension is stable and capable of carrying the nanoparticles into deeper locations of the reservoir. Thus, stability test of the nano-metal particle is needed, along with the micromodel experiments to reveal the transport and distribution of the nano-metal particles in porous media.

1.3. Aims and Objectives

This research aims to achieve the following objectives:

1. Determine the optimum concentration of nickel nanoparticle for promoting aquathermolysis under high steam temperature during CSS process.

2. Explore the performance of nickel nanoparticle in catalyzing aquathermolysis reactions at lower temperature.

3. Investigate the effect of the nickel nanoparticles' penetration depth on the final oil recovery of CSS process.

4. Investigate the catalytic effect of iron oxide nanoparticle on aquathermolysis reactions, and compare it with that of nickel nanoparticle.

5. Confirm whether water production is boosted after introducing nickel and iron oxide nanoparticle in CSS experiments, and analyze the reasons that may lead to this phenomenon.

6. Determine the polymer/surfactant recipe that can be used to stabilize nickel nanoparticle suspensions and conduct micromodel experiments to visually examine how the nickel nanoparticles are being transported in porous media.

1.4. Structure of the Thesis

This is a paper-based thesis composed of five chapters as follows:

Chapter 1 presents the research background, a brief introduction of thermal recovery as well as the problem statement, followed by the objectives and the thesis structure.

Chapter 2 presents the experimental results examining the use of nickel nanoparticles for enhancing the performance of CSS. In this chapter, a sensitivity test was first conducted to determine the optimum duration of injection period and soaking period in each CSS cycle. Then, CSS experiments were conducted under three different temperatures (150°C, 180°C and 220°C) to examine the effect of temperature on the recovery factor during CSS. After that, nickel nanoparticles were introduced by premixing them with the oil-saturated sandpack, and CSS experiments were then conducted with the presence of nickel nanoparticle under 220°C. Different nanoparticle concentrations were tested, and the optimum concentration was determined based on the test results. After obtaining the optimum nickel concentration, we applied it in the subsequent experiments at 150°C in order to check if nickel nanoparticles are

able to enhance oil production at lower temperatures. Lastly, the effect of the penetration depth of nanoparticle in the sand pack on the ultimate oil recovery was examined by placing nanoparticles in the 1/3 section of the sand pack that was close to the injection port. In addition, the control experiments, which did not involve the use of nickel nanoparticles, were repeated three times to quantify the experimental uncertainties associated with the measurement of recovery factor and viscosity.

Chapter 3 shows the results of the catalytic effect of iron oxide nanoparticle. Different concentrations of iron oxide nanoparticle were introduced into the sandpack and the CSS experiments was also conducted under 220°C. The experimental results obtained with iron oxide and nickel nanoparticle were compared. This chapter also elaborates on the detailed mechanisms leading to the phenomenon that the water production could be boosted during CSS tests that involved the use of nano-metal particles.

Chapter 4 presents static experiments to explore the optimum polymer/surfactant recipe that can be used to stabilize nickel nanoparticle solutions. Then, a series of visualization tests relying on the use of micromodels were conducted to observe the transport and distribution of nickel nanoparticles in the porous media when being injected into the sand pack. A water flooding was followed after terminating the solution injection to see if water flooding can flush away the nanoparticles.

Chapter 5 presents the conclusions of this study as well as recommendations for future work.

References

Alberta Government. Alberta's Energy Industry Overview. 2012.

Alvarez, J. and Han, S. 2013. Current overview of cyclic steam injection process. *J. Pet. Sci. Res.* **2** (3): 116-127.

Banerjee, D. Oil sands, heavy oil and bitumen: from recovery to refinery. 2012. Pennwell Corp.

Clark, P.D., Clarke, R.A., Hyne, J.B., et al. 1990. Studies on the effect of metal species on oil sands undergoing steam treatments. *AOSTRA J. Res.* **6** (1): 53-64.

Clark, P.D., and Hyne, J.B. 1983. Steam-oil chemical reactions: mechanisms for the aquathermolysis of heavy oils. *AOSTRA J. Res.* **1** (1): 15-20.

Fan, H, Liu, Y., Zhang, L. et al. 2002. The study on composition changes of heavy oils during steam stimulation process. *Fuel* **81**: 1733-1738.

Hamedi-Shokrlu, Y. and Babadagli, T. 2014a. Viscosity reduction of heavy oil/bitumen using micro- and nano-metal particles during aqueous and non-aqueous thermal applications. *J. Petro. Sci. Eng.* **119**: 210-220.

Hamedi-Shokrlu, Y. and Babadagli, T. 2014b. Kinetics of the in-situ upgrading of heavy oil by nickel nanoparticle catalysts and its effect on cyclic-steam-stimulation recovery factor. *SPE Res. Eval. Eng.* **17** (3): 355-364.

Li, X., Zhu, D., and Wang, X. 2007. Evaluation on dispersion behavior of the aqueous copper nano-suspensions. *J. Colloid Interf. Sci.* **310** (2): 456-463.

Prats, M. 1978. A current appraisal of thermal recovery. *J. Pet. Technol.* **30** (08): 1-129.

CHAPTER 2 Use of Nickel Nanoparticle for Promoting Aquathermolysis Reaction during Cyclic Steam Stimulation

A version of this chapter was presented at the 10th International Petroleum Technology Conference held in Bangkok, Thailand, 14-16 November 2016, and was also accepted for publication in *SPE Journal* (SPE-186102-PA).

Abstract

Late cycles of cyclic steam stimulation (CSS) are characterized with a decreasing heavy-oil recovery and an increasing water cut. Nickel nanoparticles can be used to promote aquathermolysis reactions between water and heavy oil in steam injection processes, thereby increasing the recovery factor. In this paper, detailed investigations were performed to determine the optimum operational parameters and answer to the following questions: (1) What is the optimum concentration of nickel nanoparticles for promoting aquathermolysis under high steam temperature? (2) Can we improve oil recovery at lower steam temperatures with the presence of nickel nanoparticles? (3) What effect does the penetration depth of nickel nanoparticles have on the final oil recovery?

CSS experiments were conducted between temperatures 150ºC and 220ºC. Steam generated under these temperatures was injected into sand packs saturated with Mexican heavy oil. Powder-form nickel nanoparticle was introduced into this process to boost the oil production. In an attempt to obtain the optimum concentration, different concentrations were tested. Next, oil sands without any nanoparticle additives were first added into the cylinder. Then, only one third of the sand pack was mixed with nickel nanoparticle near the injection port. Experiments were executed to study the effects of temperature, nickel concentrations, and nanoparticle penetration depth on the ultimate oil recovery and produced oil-water ratios after each cycle. Produced oil quality and emulsion formation were evaluated with gas-chromatography (GC) analysis, viscosity measurements, saturates-asphaltenes-resins-aromatics (SARA) test, and microscopic analysis of the effluents.

Experimental results show that the best concentration of nickel nanoparticles, which gives the highest ultimate oil recovery factor, is 0.20 wt% of initial oil in place (IOIP) under 220°C, while the nickel concentration of 0.05 wt% provides the highest recovery factors at the early stages. A lower temperature of 150°C provides a much lower recovery factor than 220°C, which is mainly due to a lower level of aquathermolysis reactions at 150°C. By analyzing the compositions of produced oil and gas samples with GC and SARA, we confirm that (1) the major reaction mechanism during the aquathermolysis reaction is the breakage of C-S bond, (2) the nickel nanoparticles can act as catalyst for the aquathermolysis reaction, and (3) the catalytic effect becomes less remarkable from cycle to cycle. One run of experiment to test the effect of particle

penetration depth revealed that nickel nanoparticle distributed near the injection port greatly contributed to the ultimate recovery factor.

2.1. Introduction

Due to a growing energy demand worldwide, unconventional resources like heavy oil and bitumen are gaining more and more attention. Developments of such resources are challenging and usually require enhanced oil recovery (EOR) techniques. Cyclic steam stimulation (CSS), also known as huff and puff involving periodical injection, soaking, and production, is considered as a common EOR method to extract heavy oil (Farouq Ali 1994). This technology has been applied worldwide successfully and it is quite effective especially for the first few cycles. However, the ultimate recovery factor of CSS varies from 10-40% of IOIP; this is comparatively lower than those of steam flooding and steam assisted gravity drainage (SAGD), which are over 50% of IOIP (Alvarez and Han 2013). Under this circumstance, high steam-oil ratio (SOR) is yielded and steam generation in the field is costly due to fuel and infrastructure cost (Hamedi-Shokrlu and Babadagli 2013). Thus, to achieve a better financial benefit, reducing the SOR and enhancing oil recovery factor are the critical problems to be tackled during the CSS process.

Steam injected into the reservoir can heat heavy oil, lower its viscosity, and increase its mobility. Another mechanism can also help to reduce heavy oil viscosity, i.e., the aquathermolysis reactions, which refer to a series of chemical reactions (Hyne 1986). Aquathermolysis describes the chemical interaction of high-temperature water with heavy oil. During this process, some of the C-S bonds of organosulfur can be broken as per the following reaction (Hamedi-Shokrlu and Babadagli 2013):

$$\text{Heavy Oil} + H_2O \rightarrow CO + H_2S + \text{Lighter Organic Compounds} \quad (1)$$

The produced CO reacts with water, transferring hydrogen from water to oil via the following water-gas-shift-reaction (Hamedi-Shokrlu and Babadagli 2014a):

$$CO + H_2O \Leftrightarrow CO_2 + H_2 \quad (2)$$

The *in-situ* production of CO_2 is also beneficial since CO2's dissolution can further reduce heavy oil viscosity. The produced hydrogen will attack the unstable and unsaturated molecules, leading

to hydrogenation upgrading reactions that can produce lighter and saturated molecules and thus reduce the viscosity of heavy oil (Clark and Hyne 1983).

According to Clark (1990a), H_2S, CO_2, H_2, CO, CH_4, and C_2-C_5 gases are generated after the heavy oil has been being treated with steam, and the amount of each gas generated differs from oil to oil. He also conducted SARA and GC tests to analyze the compositional changes of heavy oil and the molecular size of asphaltene fractions. It was concluded that the chemical reactions under steam treated conditions are mainly the breakage of a series of bonds. Among these bonds, the dissociation energy of C-S bond is less than the other bonds; thus, it is the weakest one and tends to break first. As for the breakage of this bond, the amount of H_2S generated can be an indicator of the reactivity (Hamedi-Shokrlu and Babadagli 2014).

Many metal species can act as catalyst for aquathermolysis process, such as Fe (III) and Cu (II). A lot of researches have been conducted to study such catalytic effect. Clark (1990b) first introduced a series of transition metal ionic solution to study the upgrading effect of seven types of heavy oil; viscosity reduction was observed for each type of oil. Similar work has been done by Fan et al. (2002, 2004) to prove the catalytic effect of metal species, which exist as minerals in natural reservoirs. Hamedi-Shokrlu and Babadagli (2013, 2014a-b) investigated the catalytic effect of metal particles instead of ionic solutions. They investigated the influence of particle size on promoting aquathermolysis reactions by using micron-sized and nano-sized particles. They clarified the effect of metal type, studied how to stabilize the nickel nanoparticle suspension, and examined the efficiency of the CSS process after adding nickel nanoparticle suspension as a catalyst. However, in their study, the whole experimental setup used in the CSS experiments was placed inside an oven, implying that the heat loss of sand pack to the surrounding was almost zero; thus not only the temperature, but also the pressure at different stages in the CSS experiment could quickly reach an equilibrium state and remain stable later on. However, in reality, when it came to the soaking period, pressure drop would definitely occur due to the heat loss, and in turn affect the reactions between water, oil and sand. Thus, such setup is not representative enough for simulating the actual production from a real reservoir.

In this study, a novel setup is designed to simulate the CSS process in an environment that is close to a real field scenario by placing the reactor cylinder outside the oven. We conducted a series of CSS experiments in an attempt to answer the following questions: (1) What is the

optimum concentration of nickel nanoparticles for promoting aquathermolysis under high steam temperature?; (2) Can we improve oil recovery at lower steam temperatures with the presence of nickel nanoparticles?; (3) What effect does the penetration depth of nickel nanoparticles have on the final oil recovery? To reveal the reaction kinetics involved in the aquathermolysis reactions, we performed saturates-aromatics-resins-asphaltenes (SARA) and gas-chromatography (GC) tests on the recovered oil and gas samples.

2.2. Experimental Section

2.2.1 Materials

Table 2.1 shows the properties of two Mexican heavy oil samples used in the experiment. Nickel nanoparticles (Sigma Aldrich, Canada) were used as the catalyst for aquathermolysis reactions. The size of the nanoparticles falls between 40-70 nm. Silica sand used to prepare the sand packs has a mesh size of 40-70. The average porosity of the sand packs was measured to be 34.4%. A small steel screen was installed at the inlet of the sand pack to prevent sand production problems.

2.2.2 Experimental Setup

Figure 2.1 illustrates the schematic of the setup for all the experiments. A stainless cylinder containing water was placed inside the oven for generating saturated steam. By opening the injection valve (valve #1), steam was allowed to enter the sand pack held in a 300 mL stainless cylinder. A vacuum pump was used to vacuum the collector and the cylinder for collecting evolved gas prior to each production cycle. Then, valve #2 was opened to collect the produced materials including oil, water and gas. In order to monitor the temperature/pressure changes in CSS cycles, two thermocouples were connected at the inlet and outlet of the sand pack cylinder, while one pressure transducer was installed at the outlet end of the sand pack cylinder.

2.2.3 Experimental Procedure

The general procedure for conducting the CSS experiments is briefly explained as follows. Heavy oil and sand particles were first mixed together with a slow stirring speed. The mixing process continued for 10 minutes until a homogeneous mixing was obtained. The oil sands mixtures were then introduced into a stainless steel cylinder (Swagelok, Canada) through the inlet end. To obtain a homogeneous mixture, the cylinder was vibrated as the oil sands were introduced into the cylinder. To monitor the temperature and pressure variation in the CSS

experiments, two thermocouples were installed at the inlet and outlet of the cylinder, and one pressure transducer was installed at the outlet of the cylinder. In order to generate saturated steam, 360g of water was added into the steam-generation cylinder that was placed in the oven.

Based on the experience gained by conducting repeated experiments with the same setup, the steam generation time was set at 5.5 hours. To lower down the potential heat loss, the tubing between the steam-generation cylinder and oil-sands cylinder was covered with a heating tape, and the oil-sands cylinder was wrapped with layers of aluminum foil, insulation tape, and glass wool. Steam injection was initiated by opening the valve #1. Once the steam injection was terminated, valve #1 was closed to allow for steam soaking in the sand pack. After the soaking period, the sand pack was put on production by opening valve #2. To collect the produced materials, the gathering jar and the gas collection cylinder were first vacuumed by a vacuum pump. To cool down the produced steam and water, several ice packs were wrapped around the gathering jar during the production period. Cyclic steam injection was continuing until there was little oil production. SARA tests and viscosity measurements were applied to the produced oil, while gas GC test was applied to the produced gas samples. The standard ASTM 2007-03 (2008) was followed for the measurement of saturates, aromatics, and resins, and the standard IP 143/96 (1996) was followed for the measurement of asphaltenes. The GC tests were performed with the Multiple Gas #3 GC apparatus (SRI 8610C Gas Chromatograph, SRI Instruments, USA). **Table 2.2** shows the detailed experimental scheme employed in this study.

We first conducted a series of sensitivity tests to find out the optimum durations for the injection period and soaking period. In these sensitivity tests, the field data (Sheng 2013) of CSS was used to find the optimum scheme of injecting period and soaking period. In field applications, the average injection period was around 11 days, while the soaking period was around 6.25 days. The estimated ratio of 2:1 for the injecting period and soaking period was hence implemented to simulate the field situation in this study. To determine the optimum durations for the injection period and the soaking period, a series of sensitivity tests was conducted with the Mexican heavy oil #1. At 180°C, three different scenarios were tested: (1) 30 min steam injection followed by 15 min soaking; (2) 40 min steam injection followed by 20 min soaking; and (3) 60 min steam injection followed by 30 min soaking. The scenario with the highest oil recovery factor will be used for all the remaining experiments. Oil sands with heavy oil #2 were tested from lower

temperature to higher temperature (150°C, 180°C and 220°C) to study the effect of temperature on the recovery factor.

In order to study the effect of nickel concentration on the ultimate oil recovery, different concentrations of nickel nanoparticles were used in the experiments as outlined in Table 2.2. The control experiments, which did not involve the use of nickel nanoparticles, were repeated three times to quantify the experimental uncertainties associated with the measurement of recovery factor and viscosity. These base-case experiments are numbered as Exp #6.1, Exp #6.2 and Exp #6.3 (See Table 2.2). As for the experiments with the use of nickel nanoparticles, we first added a given amount of nickel nanoparticles into heavy oil #2. The oil/nickel mixture was then mixed with sand particles resulting in the oil sands to be packed in the cylinder. Different nickel nanoparticle concentrations were tested at 220°C. After obtaining the optimum nickel concentration, we applied the optimal concentration in the subsequent experiments at 150°C in order to check if nickel nanoparticles are able to enhance oil production at lower temperatures. At last, in order to examine the effect of the penetration depth of nanoparticle in the sand pack on the ultimate oil recovery, we only placed nanoparticles in the 1/3 section of the sand pack that was close to the injection port. We used the optimum concentration of nickel nanoparticle as determined from previous experiments, and this CSS experiment was conducted at 220°C.

2.3. Results and Discussion

2.3.1 Determination of Optimum Durations of Injection Period and Soaking Period

Figure 2.2 compares the recovery factors that were obtained in Exp. #1-3. It can be seen that the highest oil recovery factor was found in Exp #2; i.e., 22.48%. In comparison with Exp #2, a lower recovery factor was obtained in Exp #3, although a 20-min longer injection period was applied in Exp #3. During the experiment, the whole experimental setup outside the oven was exposed to the room environment; heat loss may still occur even if it were already wrapped with several layers of insulation. A larger heat loss into the ambient might occur at a longer soaking time, leading to the lower oil recovery factor observed for Exp #3. In addition, with more water condensed during the injection period near the injection port, a lot of heat injected in the next steam-injection cycle would be absorbed by the injected water. Thereby, the remaining heavy oil in the deeper part of the reservoir could not be effectively heated up (Gu et al. 2014). Based on the results from the sensitivity tests, the injection duration and soaking duration used in Exp #2

was adopted in the remaining experiments. Emulsion flow was also observed during the experiments. **Figure 2.3** shows a microscopic image that was captured on the produced water/oil emulsion in Exp #2.

To examine the effect of temperature on the recovery factor during CSS, the CSS experiments were repeated for the Mexican heavy oil #2 at 150°C, 180°C, and 220°C, respectively. **Figure 2.4** shows the total recovery factors measured at different temperatures, while **Figure 2.5** shows the detailed recovery factors that were recorded at different cycles of the CSS experiments. As can been seen from Figure 2.4, an increase in temperature led to an obviously enhanced oil recovery and the highest oil recovery was achieved at 220°C. By examining Figure 2.5 it can be found that, at temperatures of 150°C and 180°C, the peak productions occurred after the second cycle while the peak production appeared right after the first cycle at 220°C. **Figures 2.6 and 2.7** show the temperature profiles and pressure profiles that were measured at the outlet end of the cylinder for Exps #4, #5, #6.1. After the first cycle, the temperature at the outlet end for Exp #4 (150°C) did not change too much, while it reached 38°C, and 50°C for Exp #5 (180°C) and Exp #6.1 (220°C), respectively. It can be observed that steam with a higher temperature led to a higher steam pressure, helping the steam penetrate more quickly into the deeper part of the sand pack. It is noted from Figure 2.6 that part of the pressure and temperature data in Exp #6.1 were lost due to malfunctions of the transducer and the thermocouples.

We attempted to measure the viscosity of the Mexican heavy oil samples that were produced from the first cycle in Exps #1-3. However, we were not able to obtain a reading as the viscosity of the produced oil sample at 25°C all exceeded the upper viscosity limit of the viscometer (DV-II+, Brookfield Engineering Lab Inc.), i.e., around 900000 cp. Thus, after being subjected to steam treatment, the Mexican heavy oil sample #1 became super heavy. The reason for the abrupt viscosity increase after steam treatment may be related to the changes in the composition and property of the heavy oil. By injecting brine into a core saturated with heavy oil, Eakin et al. (1990) observed the viscosity of the heavy oil increased 2.8 times that of the initial value, and the highest viscosity observed was even tripled. What's more, when Athabasaca oil sand was reacted with steam under 240°C for 14 days, the viscosity of the produced oil was 20% higher than its original value. Clark *et al.* (1990) attributed this phenomenon to the original oil's chemical properties and the reaction between steam and oil. Meanwhile, it is known that the water-in-oil

(W/O) emulsion will form when pure oil is mixed with water, increasing the oil viscosity. With the concentration of water droplets increasing, the friction between the continuous and dispersed phase becomes greater, leading to a higher viscosity (Tjoeng and Loro 2016). Once the water cut reaches the inversion point, the emulsion droplets will coalesce and from another continuous phase, and the viscosity will start to decrease with a further increase in the water cut (Tjoeng and Loro 2016). In this study, the same method was applied to separate the produced water and oil in all the experiments, and no water droplets could be visually noticed after separation. However, some small water droplets must still remain in the produced oil, affecting the results in the viscosity measurements to a certain extent. It is also noted that, in our study, the possible presence of air in the cylinder may also contribute to the super high viscosity of the produced oil through an oxidation mechanism, although air presence was minimized when the sand pack was tightly packed into the cylinder prior to the experiments.

We also observe an increase in the viscosity of the Mexican heavy oil sample #2 that was produced by CSS. SARA tests were respectively conducted on the original heavy oil sample #2 and the same oil sample that was produced from the first cycle in Exp #6.1. **Figure 2.8** compares the SARA test results, while **Table 2.3** provides the details mass balances of these SARA test results. Compared with the original oil, the content of both aromatics and resins increased by around 30%, the content of saturates decreased by 10%, and the content of asphaltenes experienced little change. Thus, the increased viscosity was mainly attributed to the lower content of saturates but the higher content of resins.

2.3.2 Effect of the Presence of Nickel Nanoparticle on CSS Performance

Figure 2.9 compares the recovery factors obtained from Exps #6.1-6.3 (without the use of nickel nanoparticles) and Exp #7-10 (with the use of nickel nanoparticles). The recovery factors of Exp #6.1-6.3 were 24.69%, 23.18% and 23.70%, respectively, leading to a standard deviation of 0.76% in the recovery factor. The recovery factors obtained from Exp #7 (0.50 wt% of nickel) and Exp #8 (0.20 wt% of nickel) were quite similar. Under this circumstance, a lower concentration of 0.2 wt% of nickel was definitely a superior choice compared to the concentration of 0.50 wt% from an economic point of review. Thereby, the concentration of 0.20 wt% of nickel was regarded as the optimum concentration in this study. Later in this study, this optimum concentration was also used in Exp #10 where 1/3 section of the sand pack was premixed with nickel nanoparticles. In

order to test if such nickel concentration could work at a lower temperature, we performed another run of experiment (Exp #11) using nickel concentration at 150°C.

2.3.2.1 Effect of Nickel Nanoparticle Concentration on Oil Recovery

Figure 2.10 shows the detailed oil recovery factors that were measured at different cycles of CSS experiments with the use of different nickel concentrations at 220°C. It can be seen from Figure 2.10 that the highest recovery factor was always obtained in the first cycle, followed by a general decline trend in the later cycles of Exps #6.1-9. Such decrease in the recovery factor in the later cycles can be well attributed to the decreased relative permeability of oil in the sand pack near the injection port. With water injected into the sand pack in each cycle, the water saturation near the injection port kept increasing as a function of time, which in turn reduced the relative permeability of oil. As for the experiments with nickel concentrations of 0.05 wt% and 0.2 wt%, it is interesting to note that cycle #5 provided a higher recovery factor than cycle #4, which was then followed by a decrease in the recovery factor again. It is also noted from Figure 10 that the nickel concentration of 0.05 wt% provided a higher recovery factor in the first and second cycles of CSS experiments compared to the other two concentrations (0.50 wt% and 0.20 wt%); later in the paper, we elaborate on the reasons leading to such increase in the oil recovery factor provided by the nickel concentration of 0.05 wt%. But, in the later cycles, the nickel concentration of 0.05 wt% tended to yield the lowest recovery factors among the three concentrations considered.

Figure 2.11 shows the viscosity-temperature relations for heavy oil samples that were produced from the different stages in the recovery experiments. As previously mentioned, the viscosity of produced oil may be affected by the existence of water droplets. Thus, to test the consistency of the viscosity measurements, we measured the viscosity of three oil samples produced from cycle #1 of the base-case experiments (Exp #6.1-6.3). **Figure 2.11a** presents the comparative results, showing that the viscosity of the three oil samples collected from cycle #1 of the three base-case experiments was quite similar to each other. This further validates the consistency and repeatability of our experiments. It can be also observed from Figure 2.11a that the oil sample produced by the steam-only recovery experiments exhibited a higher viscosity than the original oil sample.

We also measured the viscosity of the oil samples produced from the cycle #1 of Exp #7, Exp #8, and Exp #9. Exp #7-9 did use difference concentrations of nickel nanoparticles. As can be seen from **Figure 2.11b**, Exp #7, Exp #8 and Exp #9 produced less viscous oils in the first cycle than Exp #6.1. This indicates that the produced heavy oil did go through an upgrading process due to the aquathermolysis reactions. But the comparison of Figures 2.10 and 2.11b indicates that, in the first cycle of Exps #7-9, such decrease in the viscosity of the produced oil was not directly converted to an increase in the oil recovery. This might be due to the fact that the oil-phase mobility (oil-phase permeability divided by oil viscosity) was mainly controlled by the high relative permeability as the initial oil saturation close to the injection port was high. As CSS cycle proceeded, the water saturation close to injection port became higher and higher. Also, the property of produced oil might also change due to the change in the aquathermolysis-reaction kinetics under different *in-situ* conditions. As can be seen from **Figure 2.11c**, the viscosity of the heavy oil produced after cycle #2 of Exp #8 was found to be much lower than the heavy oil produced after cycle #2 of Exp #9; this can well explain why Exp #8 provided a much higher recovery in the later cycles than Exp #9.

Figure 2.12 shows the GC analysis results for the gas samples produced in the first cycle of Exps #6, #8, and #9. Also shown in Figure 2.12 are the GC analysis results on the gas sample produced in cycle #3-6 of Exp #9. According to Clark et al. (1990b), transition metals can act as catalyst for aquathermolysis. During the aquathermolysis reactions, the energy needed for the cleavage of C-S bond of organosulphur compounds is the lowest, such that the amount of hydrogen sulfide generated serves as a good indication of the level of aquathermolysis reactions. It can be observed from Figure 2.12 that hydrogen sulfide was detected from the gas sample gathered from the first cycle for both Exp #8 and Exp #9, but the weight percentages of hydrogen sulfide were found to be different for the two runs of experiments. The weight percentage of hydrogen sulfide was found to be 1.1 vol% in Exp #9, which is much higher than 0.5 vol% that was detected in Exp #8. This implies that, as for the first cycle, the upgrading effect of the nickel nanoparticle with a concentration of 0.05 wt% was more significant than that with 0.20 wt%, resulting in a lower oil viscosity and hence a higher recovery factor. Such conclusion is also consistent with previous research (Hamedi-Shokrlu and Babadagli 2014a). According to their results, the collisions and aggregation of nickel nanoparticle due to Brownian motion could become stronger at a higher concentration because of the very small size of the nanoparticles.

Thus, the 0.05 wt% loading might provide a more even dispersion of the nanoparticles, leading to less aggregation of nanoparticles and hence a higher surface to volume ratio. Being more exposed to the surrounding environment, the nanoparticles could provide a higher reactivity in promoting the aquathermolysis reactions.

As mentioned before, the nickel concentration of 0.05 wt% led to a higher oil recovery factor in cycle #1 and cycle #2 of Exp #9. However, as can be seen from Figure 2.11b, there is little difference in the viscosity of heavy oils produced in the first cycles of Exp #8 and Exp #9, and this difference was even within the experimental error. Other factors must have contributed to the observed increase in the oil recovery factor due to the use of the nickel concentration of 0.05 wt%. We recall that during the experiments, the time to collect the same amount of gas in the first cycle of Exp #9 was much shorter that that needed in Exp #10. This indicates that the amount of gas produced by the 0.05 wt% nickel concentration in the first cycle was much larger than that by 0.20 wt% nickel concentration. The gas generated from the aquathermolysis reactions can provide an effective solution-gas-drive mechanism for enhancing oil production. Furthermore, Figure 2.12 shows that no hydrogen sulfide was detected in the last four cycles of Exp #9 (0.05 wt%), indicating that the aquathermolysis reactions became much less active in these later cycles.

In addition, a series of SARA tests were also applied to the produced oils from cycle #1 in Exp #7 (0.50 wt% nickel nanoparticle), Exp #8 (0.20 wt% nickel), and Exp #9 (0.05 wt% nickel). These SARA tests can help analyze the compositional changes of crude oil after nickel exposure. **Figure 2.13** show the SARA test results for the original heavy oil #2 as well as the oil samples produced in cycle #1 from Exp #6.1 (base case), Exp #7 (0.50 wt% nickel), Exp #8 (0.20 wt% nickel), and Exp #9 (0.05 wt% nickel). Figure 2.13 shows, as compared with the oil obtained in Exp #6.1, a significant increment in the saturates content, together with a decrease in the resins content, could be noticed for all the oil samples after nickel exposure. But, the variation trend in the aromatics/asphaltenes content was not obvious. Heavy oil viscosity is a comprehensive reflection of the four fractions in the sample, and many researches have proved that the interplay of asphaltene and resin has the most significant effect on oil viscosity (Pierre et al. 2004). Thus, the similar viscosity of the produced oils might be the consequence of the interplay of asphaltenes and resins content. It is also noted that the oil from Exp #9 (0.05 wt% nickel)

showed the highest increment in saturates fraction. Such finding is consistent with the gas GC results that a concentration of 0.05 wt% of nickel nanoparticle generated the highest amount of hydrogen sulfide, confirming a better upgrading effect provided by this concentration.

Based on these experimental results, it is obvious that the nickel nanoparticles did function as a catalyst for promoting aquathermolysis reactions and could improve oil recovery factor. In this study, the optimum concentration of nickel nanoparticle giving the maximum ultimate recovery factor was 0.20 wt%. The viscosity measurements on the recovered oil samples showed that the catalytic effect of 0.20 wt% nickel concentration lasted for at least 7 cycles, albeit the catalytic effect became less obvious as time elapses. In comparison, a lower nickel concentration provided a strong catalytic function in the first two cycles; however, its catalytic effect diminished quickly in the later cycles. Some possible reasons may contribute to the reduced catalytic effect: (1) certain amount of nickel nanoparticles were produced along with oil and water; and (2) the sintering-induced shrinkage in the particle size of nickel nanoparticles would lead to a lower reactivity (Moon et al. 2009)

2.3.3.2 Effect of Nickel Nanoparticle Addition on Water Production

In comparison to the steam only case, we also noticed an increase in the water production when nickel nanoparticles were present in the porous media. **Figure 2.14** shows the water amount produced in each cycle of Exps #6.1-9. After nickel nanoparticles were introduced into the sand pack, water production started to pick up from the first cycle. Therefore, in addition to the increase in the oil-phase mobility due to the promoted aquathermolysis reactions, the water-phase relative permeability may also be increased and contribute to a higher water production. But such increased water production might be also related to the increased reservoir pressure due to the gas generated by the aquathermolysis reactions. This observation is consistent with previous experiments reported by Farooqui et al. (2015). Further research is needed to clarify the exact mechanisms underlying the observed increases in the oil and water productions.

2.3.3.3 Effect of Temperature on the Performance of Nickel Nanoparticles

We also did a run of experiment with the use of nickel nanoparticles at a lower temperature of 150°C in order to test if such aquathermolysis reactions can help to promote the oil production at lower temperatures. As shown in **Figure 2.15**, the recovery factor from the first cycle in Exp #11 after introducing 0.20 wt% nickel was improved significantly compared with Exp #4. However,

this kind of improvement disappeared from the second cycle, and finally led to a lower ultimate recovery factor. Deficient reactivity of nickel under a low temperature may explain this result. After catalyzing aquathermolysis for the first cycle, nickel in this system may not be able to keep as active as before under lower temperatures, and thus the insufficient reactivity result in a lower recovery factor.

2.3.3.4 Effect of Nickel Penetration Depth on Oil Recovery

To test the influence of nickel nanoparticle penetration on the recovery performance, we deliberately placed the nickel nanoparticles only in the first 1/3 section of the sand pack in Exp #10, and repeated the CSS experiments. As shown in Figure 2.8, compared with the steam-only case (Exp #6), Exp #8 yielded an improvement of 11.22% in the ultimate oil recovery, while Exp #10 provided an improvement of 8.02% in the ultimate oil recovery with the use of the same nickel concentration. It is noted that the recovery factor obtained from Exp #10 was only 3.20% lower than that obtained from Exp #9, indicating that the nickel nanoparticles that were placed close to the injection port contributed the most to the enhanced oil production. **Figure 2.16** further shows the recovery factors measured at different cycles of Exp #8 and Exp #10. We can see from Figure 2.15 that there were large differences in the recovery factors in the last few stages of Exp #8 and Exp #10. This suggests that the nanoparticles placed in the deeper part of the reservoir became activated at later stages, contributing to the higher oil recovery at later cycles. **Figure 2.17** shows the viscosity of oil samples that were produced at different cycles of CSS Exp #8 and Exp #10. Figure 2.15 indicates that the produced-oil viscosity in the first cycle of Exp #10 was similar to that in the first cycle of Exp #8. But, the produced-oil viscosity in the later cycles of Exp #10 was much higher than in the later cycles of Exp #8. Figure 2.16 well explains the resulting recovery profiles as shown in Figure 2.15. In summary, the contribution of nickel nanoparticles for improving recovery factor mainly originated from the nanoparticles that were distributed near the injection port. Nonetheless, the nickel nanoparticles should be placed deeper into the reservoir to achieve a better oil recovery in the long run.

2.4. Conclusions

We have conducted a series of experiments to investigate the use of nickel nanoparticle in promoting the aquathermolysis reactions in CSS. The following conclusions can be obtained:

(1) Nickel nanoparticle can act as catalyst for aquathermolysis during CSS process and break C-S bond effectively. However, the catalytic effect of nickel tends to decrease with time, and even disappear at the very late stages. This might be related to the decrease in the nickel concentration in the sand pack in later cycles;

(2) For the Mexican heavy oil sample #2 used in this study, a nickel nanoparticle concentration of 0.05 wt% augmented the recovery most significantly in the early stages. A nickel nanoparticle concentration of 0.20 wt% applied at 220°C was found to be the optimum concentration yielding the highest overall recovery factor because the catalytic effect of nickel could last for a longer time at a higher nickel nanoparticle concentration;

(3) After introducing nickel nanoparticle into the sand pack, the increase in oil recovery was also accompanied by a dramatic increase in the water production;

(4) The use of nickel nanoparticles at 150°C had a certain upgrading effect at the very early stage of the CSS process; however, it could not improve the ultimate oil recovery in this study;

(5) The contribution of nickel nanoparticle for improving recovery factor mainly originated from the nanoparticles that were distributed near the injection port. The nickel nanoparticles should be placed deeper into the reservoir to achieve a better oil recovery in the long run.

Acknowledgements

This research was conducted under Prof. Tayfun Babadagli's NSERC Industrial Research Chair in Unconventional Oil Recovery (industrial partners are Petroleum Development Oman, Total E&P Recherche Développement, SIGNa Oilfield Canada, CNRL, SUNCOR, Touchstone Exploration, Sherritt Oil, PEMEX, Husky Energy, Saudi Aramco, Devon. and APEX Eng.) and NSERC Discovery Grant (No: RES0011227 and NSERC RGPIN 05394). We gratefully acknowledge these supports.

References

Alvarez, J. and Han, S. 2013. Current overview of cyclic steam injection process. *J. Pet. Sci. Res.* **2** (3): 116-127.

Clark, P.D., Clarke, R.A., Hyne, J.B., et al. 1990a. Studies on the chemical reactions of heavy oils under steam stimulation conditions. *AOSTRA J. Res.* **6** (1): 29-39.

Clark, P.D., Clarke, R.A., Hyne, J.B., et al. 1990b. Studies on the effect of metal species on oil sands undergoing steam treatments. *AOSTRA J. Res.* **6** (1): 53-64.

Clark, P.D., and Hyne, J.B. 1983. Steam-oil chemical reactions: Mechanisms for the aquathermolysis of heavy oils. *AOSTRA J. Res.* **1** (1): 15-20.

Eakin, B.E., Mitch, F.J., and Hanzlik, E.J. 1990. Oil property and composition changes caused by water injection. Paper SPE-20738 presented at the 65th SPE Annual Technical Conference and Exhibition, New Orleans, Louisiana, 23-26 September.

Fan, H, Liu, Y., Zhang, L. et al. 2002. The study on composition changes of heavy oils during steam stimulation process. *Fuel* **81**: 1733-1738.

Fan, H., Zhang, Y., and Lin, Y. 2004. The catalytic effects of minerals on aquathermolysis of heavy oils. *Fuel* **83**: 2035-2039.

Farouq Ali, S.M. 1994. CSS – Canada's super strategy for oil sands. *J. Can. Petro. Tech.* **33** (9):16-19.

Farooqui, J., Babadagli, T., and Li, H. 2015. Improvement of the recovery factor using nano-metal particles at the late stages of cyclic steam stimulation. Paper SPE-174478-MS presented at the SPE Canada Heavy Oil Technical Conference, Calgary, Alberta, Canada, 9-11 June.

Gu, H., Cheng, L., Huang, S. et al. 2015. Steam injection for heavy oil recovery: Modelling of wellbore heat efficiency and analysis of steam injection performance. *Energ. Convers. Manage.* **97**: 166-177.

Hamedi-Shokrlu, Y. and Babadagli, T. 2013. In-Situ upgrading of heavy oil/bitumen during steam injection by use of metal nanoparticles: a study on in-situ catalysis and catalyst transportation. Paper SPE-146661 presented at the SPE Annual Technical Conference and Exhibition, Denver, Colorado, 30 October -2 November.

Hamedi-Shokrlu, Y. and Babadagli, T. 2014a. Viscosity reduction of heavy oil/bitumen using micro- and nano-metal particles during aqueous and non-aqueous thermal applications. *J. Petro. Sci. Eng.* **119**: 210-220.

Hamedi-Shokrlu, Y. and Babadagli, T. 2014b. Kinetics of the in-situ upgrading of heavy oil by nickel nanoparticle catalysts and its effect on cyclic-steam-stimulation recovery factor. *SPE. Res. Eval. Eng.* **17** (3): 355-364.

Hyne, J.B. 1986. Aquathermolysis - A synopsis of work on the chemical reactions between water (steam) and heavy oil sands during simulated steam stimulation. Synopsis report No.50, AOSTRA contracts No. 11, 103, 103B/C.

Moon, Y., Lee, J., Kim, J., et al. 2009. Sintering kinetic measurement of nickel nanoparticle agglomerates by electrical mobility classification. *Current Applied Physics* **9** (5): 928-932.

Pierre, C., Barre, L., Pina, A., et al. 2004. Composition and heavy oil rheology. *Oil Gas Sci. Tech*. **59** (5): 489-501.

Sheng, J.J. 2013. *Enhanced oil recovery field case studies*. Gulf Professional Publishing.

Tjoeng, A.Y., and Loro, R. 2016. Viscosity modelling of Pyrenees crude oil emulsions. Paper SPE 182326 presented in the Asia Pacific Oil & Gas Conference and Exhibition, Perth, Australia. 25-27 October.

Tables and Figures

Oil	API	Density at 25°C (kg/m^3)	Saturates wt%	Aromatics wt%	Resins wt%	Asphaltenes wt%	Viscosity at 25°C (cp)
Mexican heavy oil #1	_	992.8	_	_	_	_	159000
Mexican heavy oil #2	10.75	987.9	31.93	18.92	24.36	24.57	45590

Table 2.1 Properties of heavy oil samples used in Chapter #2.

Exp. No	Temperature (°C)	Original oil viscosity (cp)	Injection duration (min)	Soaking duration (min)	Nickel concentration (g/g, wt%)	Relative nickel penetration depth (m/m)
1	180	159000	30	15	0	0
2	180	159000	40	20	0	0
3	180	159000	60	30	0	0
4	150	45990	40	20	0	0
5	180	45990	40	20	0	0
6.1	220	45990	40	20	0	0
6.2	220	45990	40	20	0	0
6.3	220	45990	40	20	0	0
7	220	45990	40	20	0.50	1
8	220	45990	40	20	0.20	1
9	220	45990	40	20	0.05	1
10	220	45990	40	20	0.20	1/3
11	150	45990	40	20	0.20	1

Table 2.2 Experimental schemes used in Chapter #2.

*Note: The relative nickel penetration depth refers to the length of the sand pack premixed with nickel nanoparticles relative to the total length of the sand pack.

	Saturates, wt%	Aromatics, wt%	Resin, wt%	Asphaltene, wt%
Original heavy oil #2	31.93	18.92	24.36	24.57
Exp #6.1 (Steam only)	20.84	24.99	30.24	23.80
Exp #7 (0.50 wt%)	20.92	25.89	25.89	23.02
Exp #8 (0.20 wt%)	24.68	22.95	24.83	27.45
Exp #9 (0.05 wt%)	27.45	22.16	26.28	24.80

Table 2.3 SARA test results for the original heavy oil #2 and oil samples that were collected from the first cycles of Exp #6.1, #7, #8, and #9 in this study.

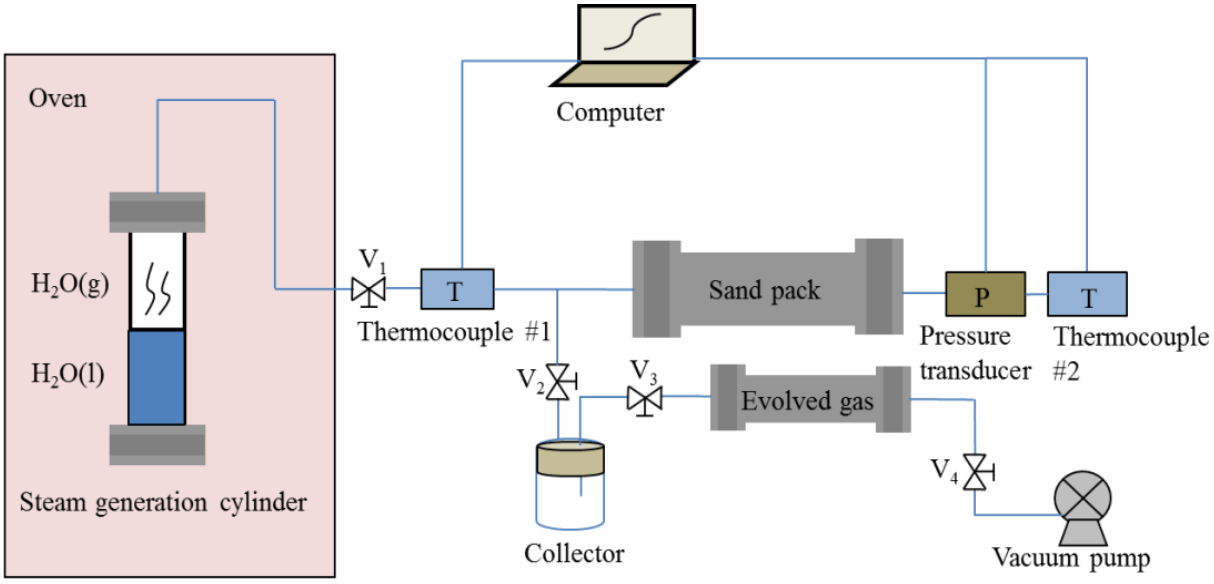

Figure 2.1 Experiment setup used for conducting the CSS experiments with the use of nanoparticles.

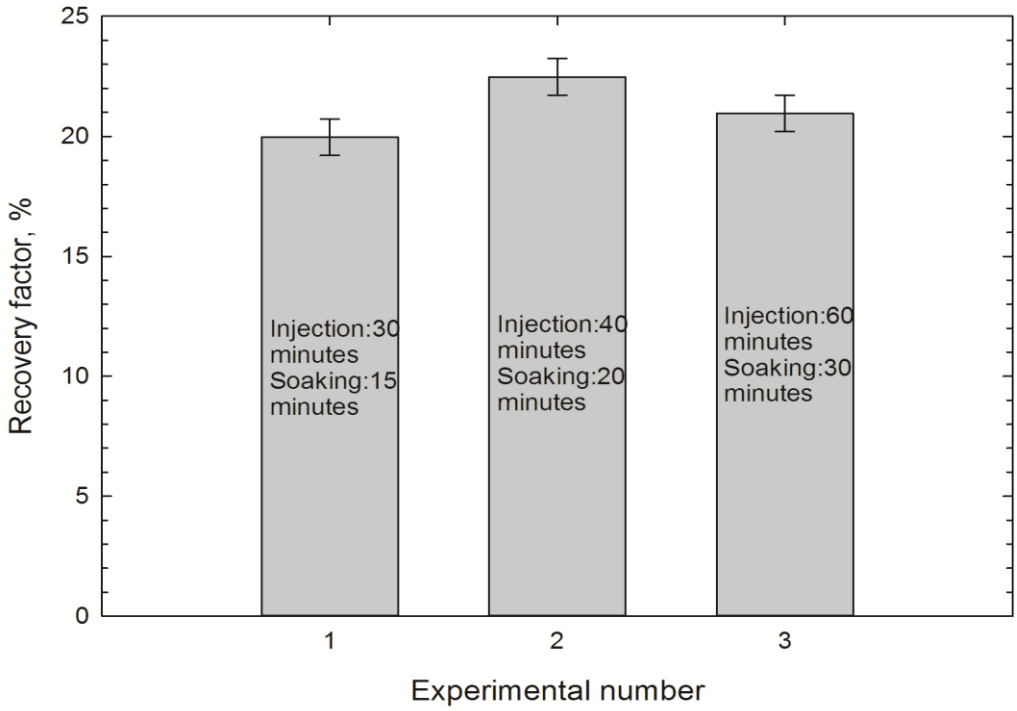

Figure 2.2 Effect of injection durations and soaking durations on the oil recovery factor for Mexican heavy oil sample #1.

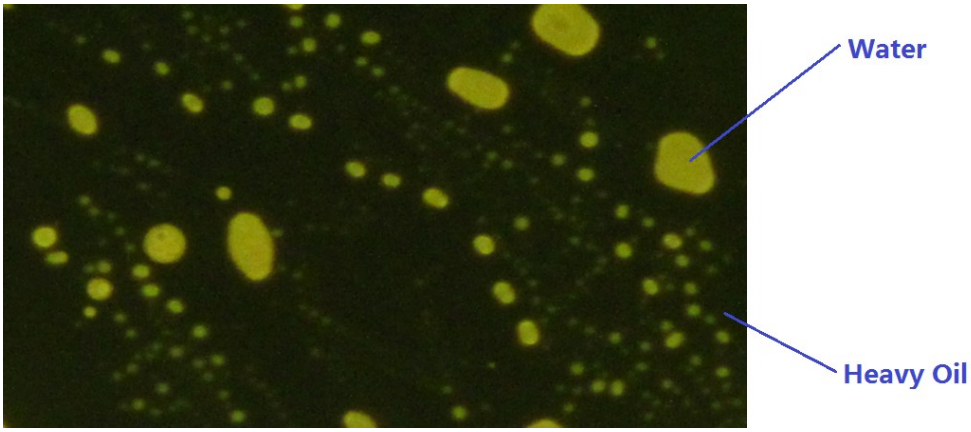

Figure 2.3 Microscopic image of a produced oil sample from cycle #1 of Exp #6.

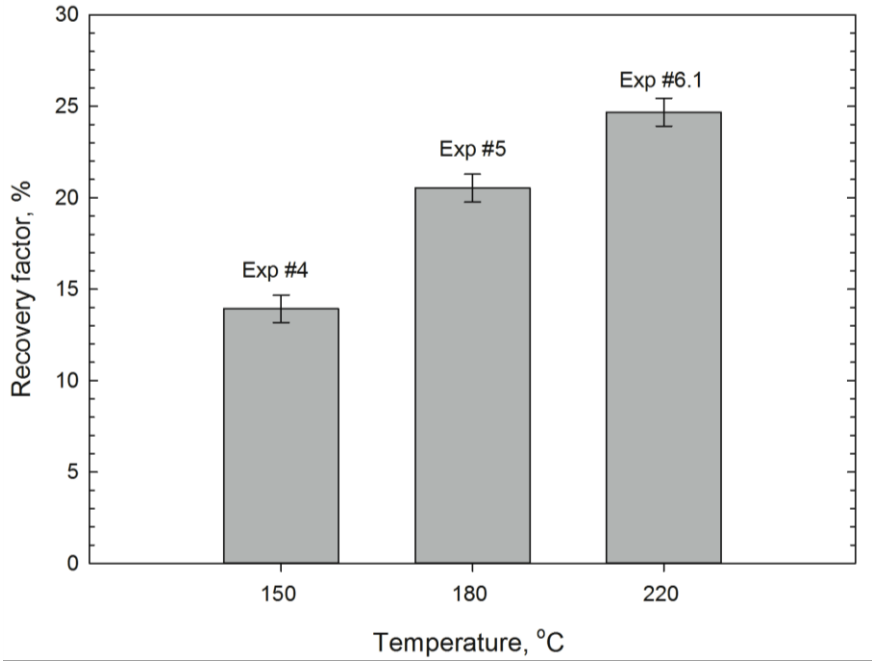

Figure 2.4 Recovery factors measured by CSS tests for the Mexican heavy oil samples #2 under temperatures of 150°C, 180°C and 220°C.

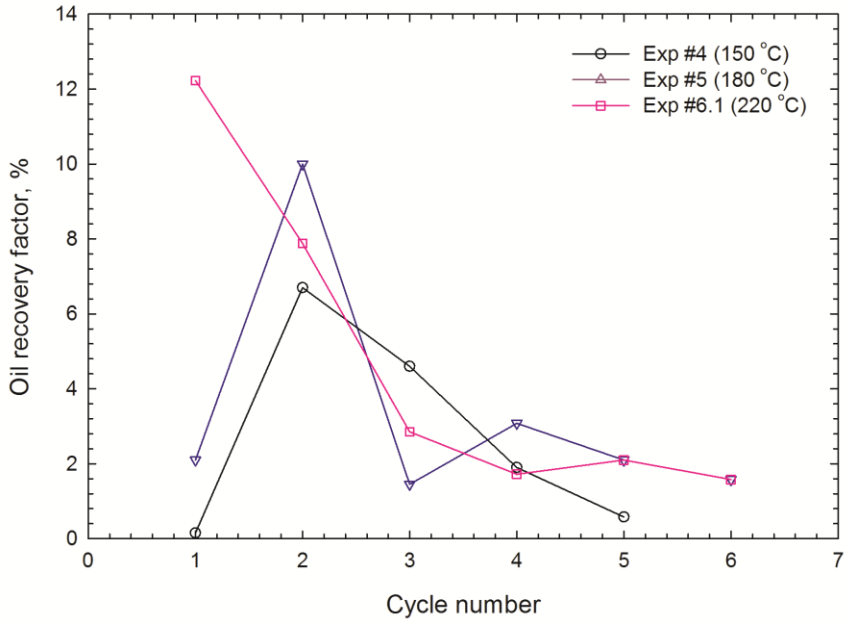

Figure 2.5 Oil recovery factors that were measured at different cycles under the temperatures of 150°C, 180°C and 220°C.

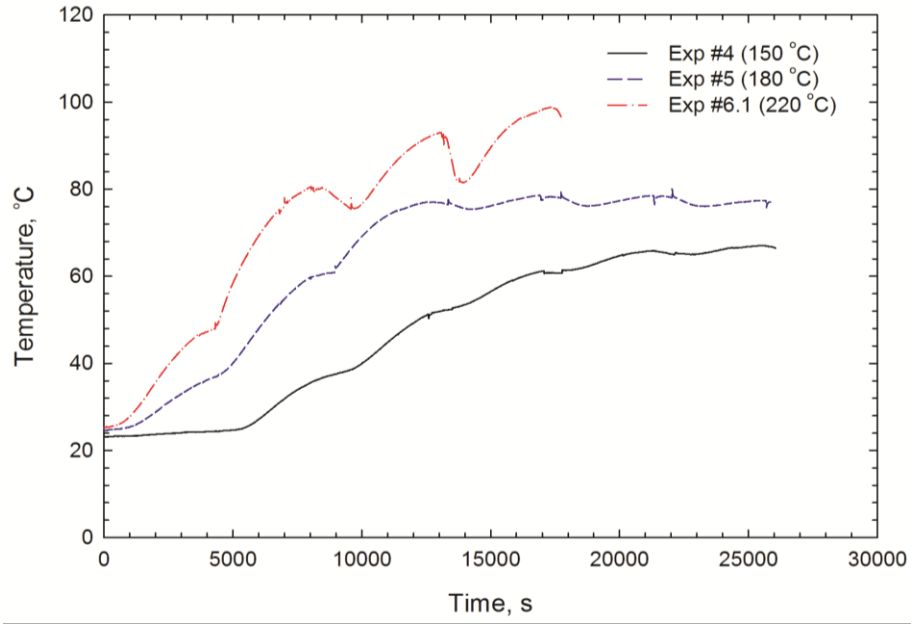

Figure 2.6 Temperature profiles at the outlet end of the cylinder recorded under different temperatures.

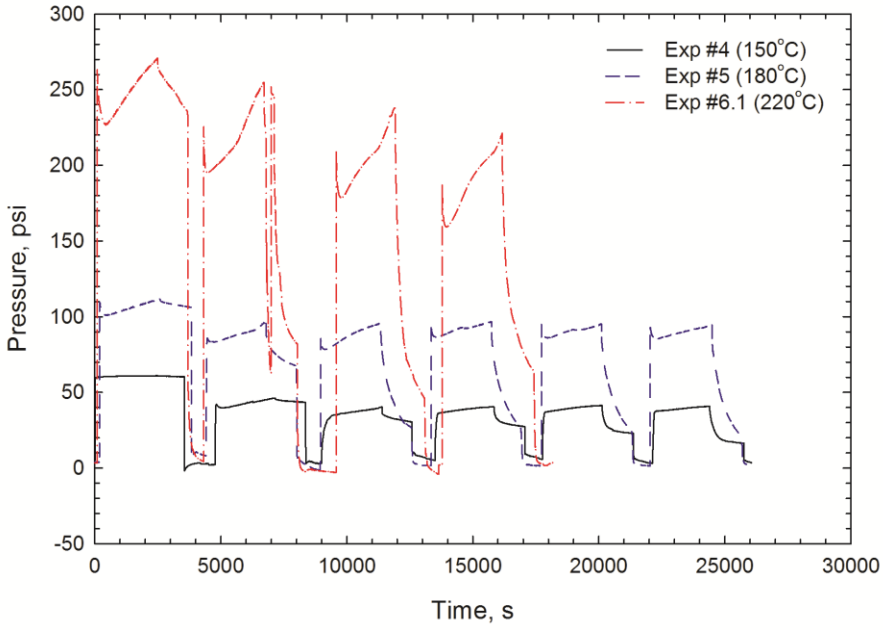

Figure 2.7 Variations of outlet pressure in the sand pack as a function of time recorded in the CSS experiments under different temperatures.

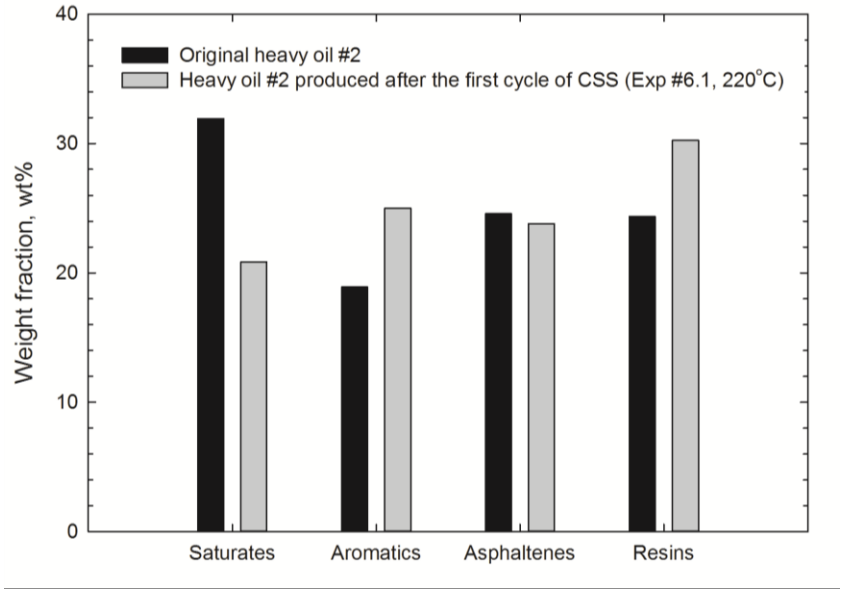

Figure 2.8 SARA analysis results that were measured for the original heavy oil sample #2 and heavy oil sample #2 after CSS experiments.

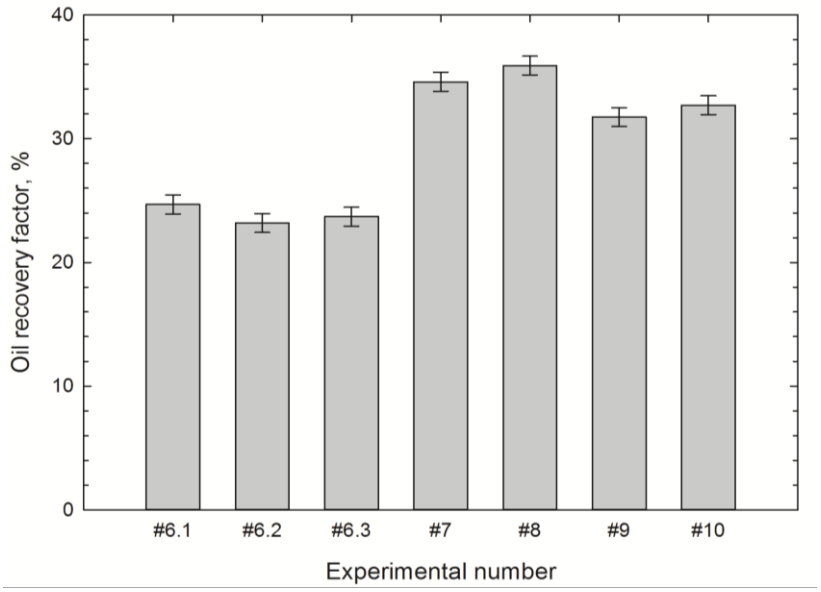

Figure 2.9 Ultimate oil recovery factors that were measured in Exp #6.1-6.3 (base cases), Exp #7 (0.50 wt% of nickel), Exp #8 (0.20 wt% of nickel), Exp #9 (0.05 wt% of nickel) and Exp #10 (0.20 wt% of nickel, 1/3 penetration depth) at 220°C.

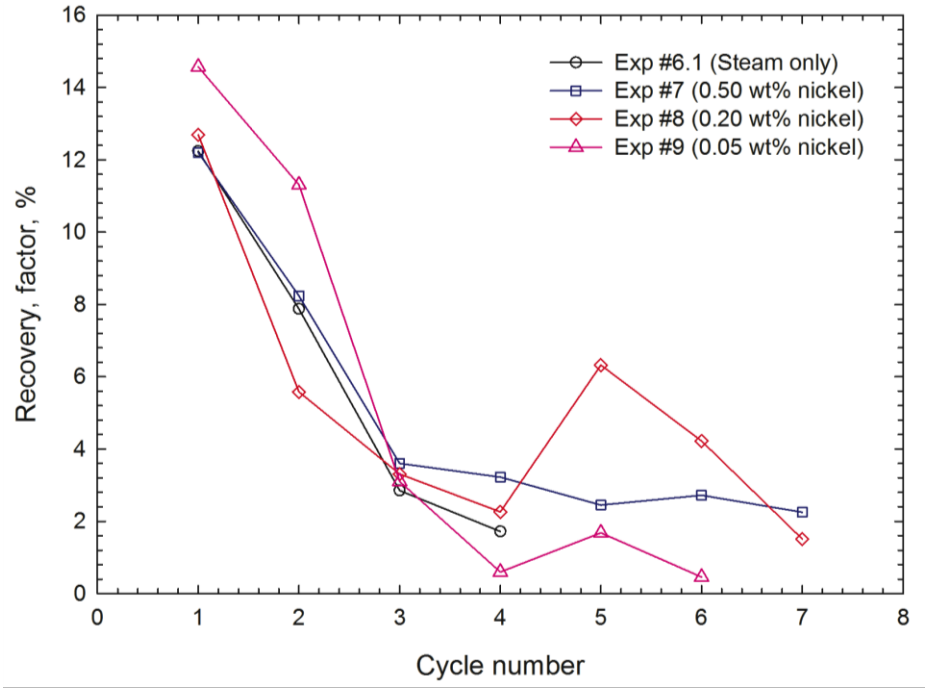

Figure 2.10 Oil recovery factors that are measured at different cycles of CSS experiments with the use of different nickel concentrations at 220°C.

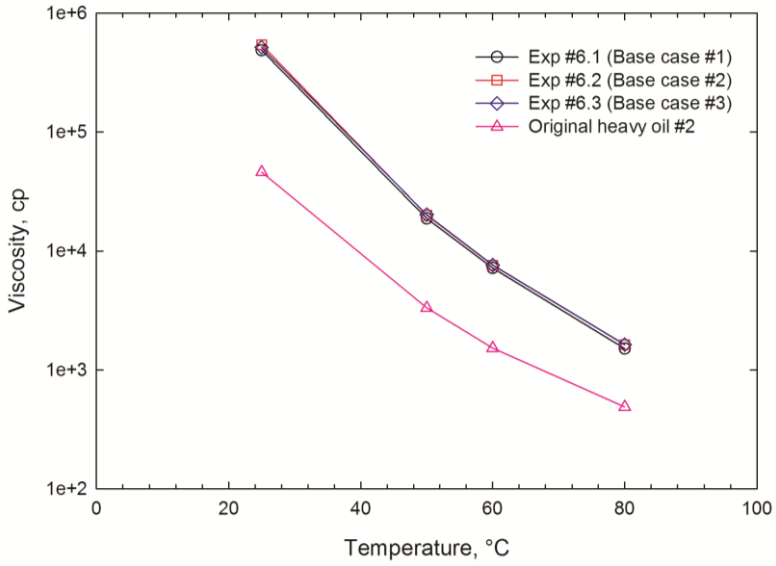
Exp #6.1 (Base case #1)
Exp #6.2 (Base case #2)
Exp #6.3 (Base case #3)
Original heavy oil #2
Viscosity, cp
Temperature, °C
1e+6
1e+5
1e+4
1e+3
1e+2
0
20
40
60
80
100

(a)

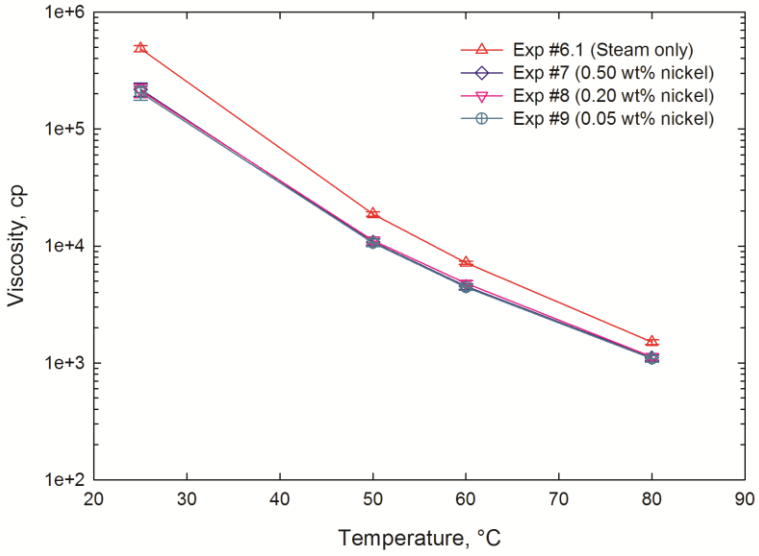
Exp #6.1 (Steam only)
Exp #7 (0.50 wt% nickel)
Exp #8 (0.20 wt% nickel)
Exp #9 (0.05 wt% nickel)
Viscosity, cp
Temperature, °C
1e+6
1e+5
1e+4
1e+3
1e+2
20
30
40
50
60
70
80
90

(b)

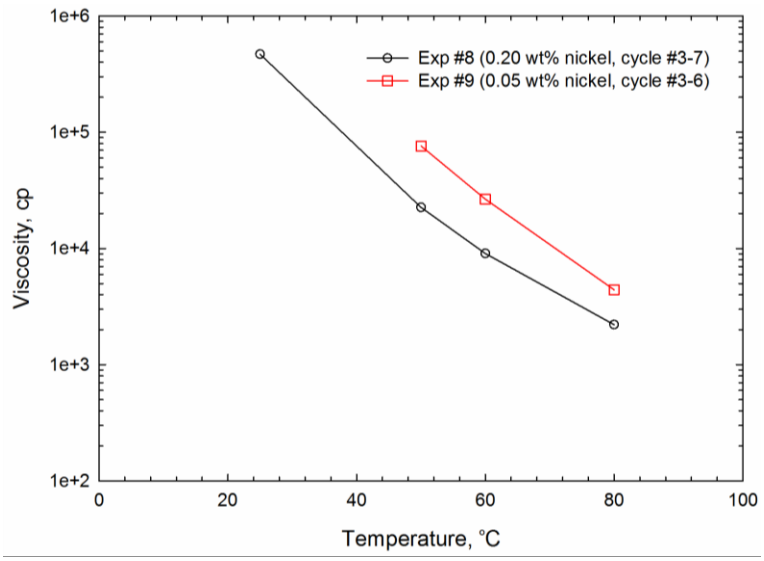

(c)

Figure 2.11 Viscosity of the oil samples that were collected at different cycles of CSS experiments: (a) cycle #1 of base-case experiments #6.1-6.3; (b) cycle #1 of Exps #6, #8 and #9; (c) cycles #3-7 of Exp #8 and cycles #3-6 of Exp #9.
*Note: the viscosity of heavy oil produced in the cycles #3-6 of Exp #9 in Figure c exceeded the maximum viscosity (i.e., 900,000 cp) of the viscometer.

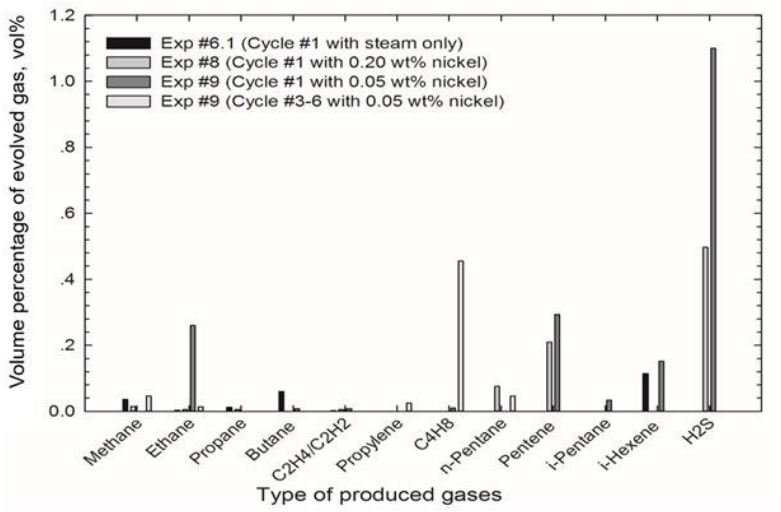

Figure 2.12 GC analysis results for the gas samples that were collected during cycle #1 from Exp #6.1 (base case) and Exp #8-9 (with nickel), and cycle #3-6 in Exp #9.

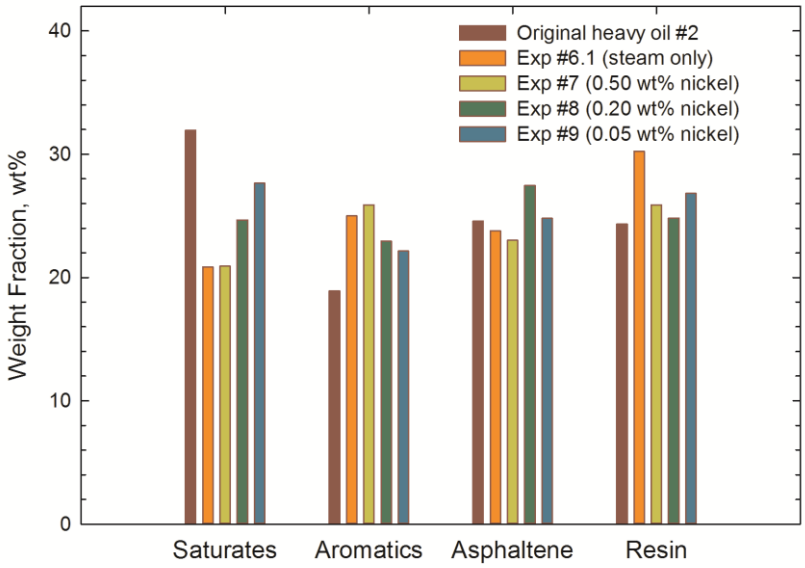

Figure 2.13 SARA test result for original heavy oil #2 and produced oil collected in cycle #1 from Exp 6.1 (base case #1), Exp 7 (0.50 wt% nickel), Exp #8 (0.20 wt% nickel), Exp #9 (0.05 wt% nickel).

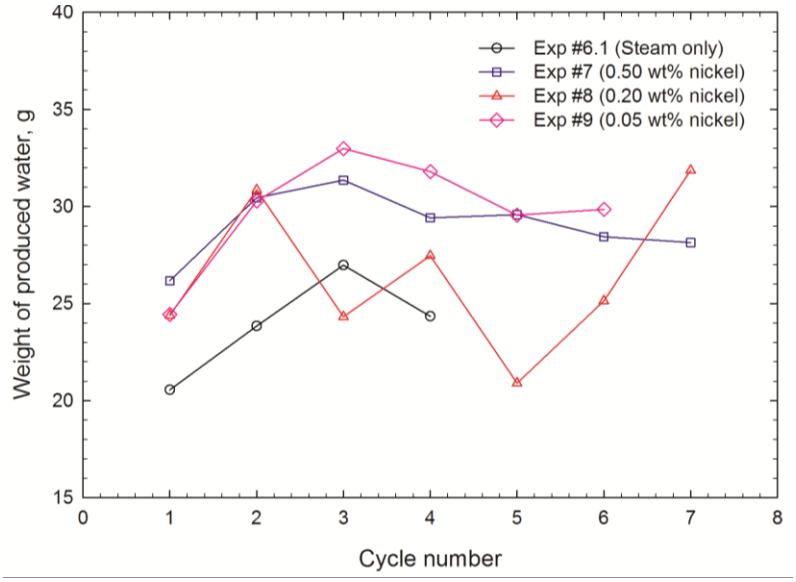

Figure 2.14 Weight of water produced at different cycles of CSS experiments.

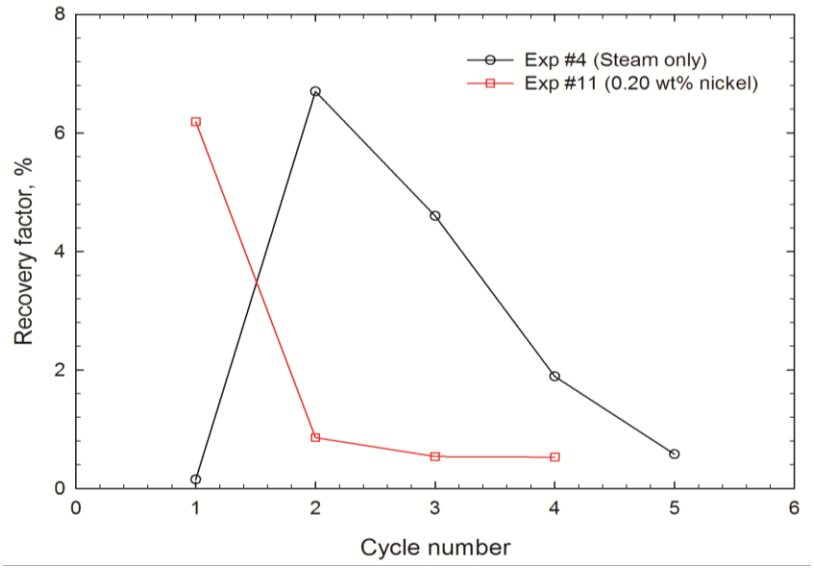

Figure 2.15 Oil recovery factor obtained from each cycle from Exp #6.1 (steam only) and Exp #11 (0.20 wt% nickel).

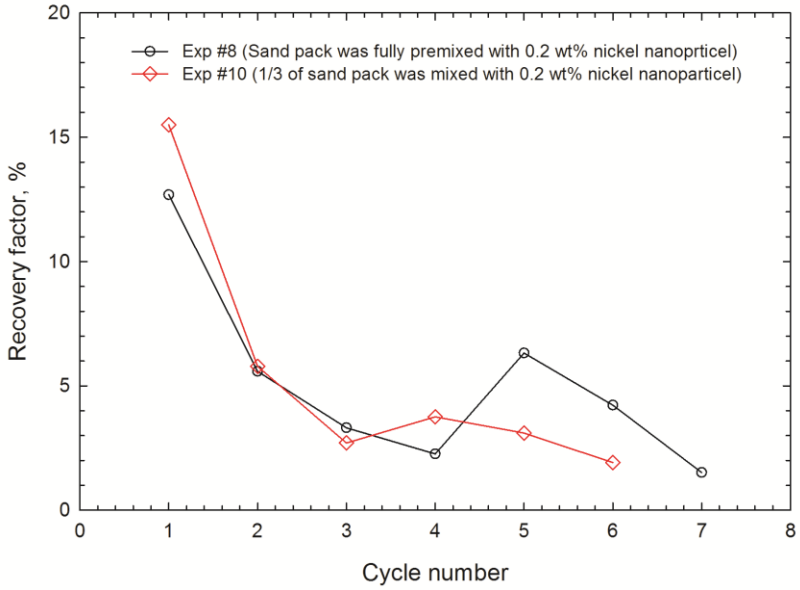

Figure 2.16 Recovery factors measured at different cycles of CSS experiments.

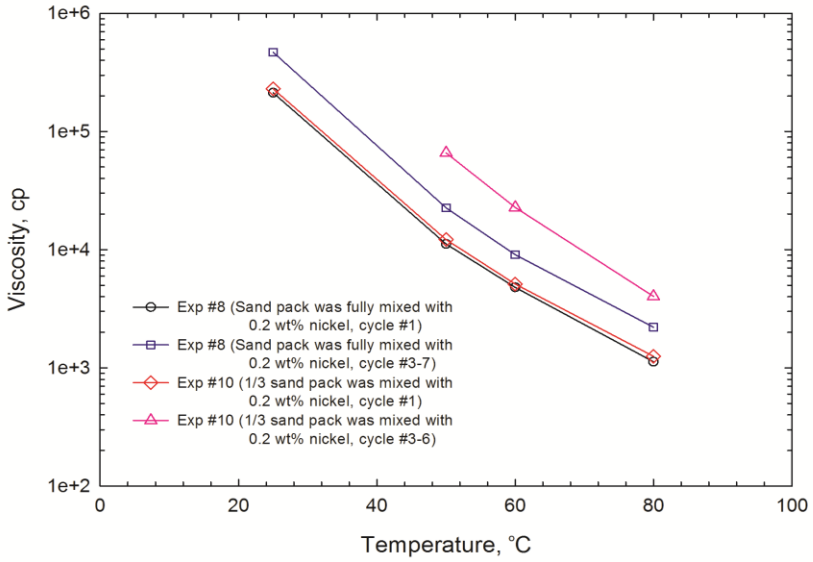

Figure 2.17 Viscosity of oil samples that were measured at different cycles of CSS experiments.

*Note: viscosity of heavy oil produced in cycles #3-6 of Exp #10 exceeded the maximum viscosity (900000 cp) of the viscometer.

CHAPTER 3 Catalytic-Effect Comparison between Nickel and Iron Oxide Nanoparticles during Aquathermolysis-Aided Cyclic Steam Stimulation

A version of this chapter is submitted to *SPE Reservoir Evaluation & Engineering, 2017.*

Abstract

Cyclic steam stimulation (CSS) has been proved to be an effective technique to boost the oil production, and a lot of metal species can act as catalyst for aquathermolysis reactions during this process. In this paper, a series of CSS experiments with and without nano-metal particles were conducted under 220°C to compare the performance of nickel (Ni) and iron oxide (Fe_2O_3) nanoparticles in promoting the aquathermolysis reactions in CSS; different loadings of nano-metal particles were tested in the CSS experiments. During the experiments, we monitor the variations of oil recovery factor, oil viscosity, gas composition and water production. The experimental results show that both nickel and iron oxide nanoparticles can act as catalyst for aquathermolysis reactions and reduce the viscosity of heavy oil. However, their catalytic effect differs dramatically. Nickel nanoparticle can break C-S bond more effectively than iron oxide nanoparticle, together with achieving a higher ultimate oil recovery factor of CSS. Along with the boosted oil production, the water production was also increased from the very first cycle after introducing the nano-metal particles in CSS. The gas chromatography (GC) analysis and the pressure data recorded during each soaking period revealed that a higher amount of evolved gas including alkenes and hydrogen sulfide was generated in the early stage, increasing reservoir pressure and forcing more condensed water produced from the sandpack.

3.1 Introduction

The international definition of heavy oil was first discussed at the World Petroleum Congress in 1980 (Banerjee 2012). Since then, heavy oil began to play an increasingly important role in the energy industry. Various types and sizes of heavy oil deposits are found in several countries, such as Canada, United States, China, and Venezuela (Banerjee 2012). To overcome its high viscosity problem, several thermal extraction techniques have been employed to reduce the viscosity of heavy oil and improve its mobility (Franco et al. 2016). Among them, steam-assisted gravity drainage (SAGD) and cyclic steam stimulation (CSS) are the most widely applied thermal techniques for enhancing heavy oil recovery.

It has been proved that when high temperature steam is injected into the reservoir, the reduction of viscosity is not only a physical process but is also related to a series of chemical

reactions known as aquathermolysis, which refers to a series of chemical reactions between high-temperature water and heavy oil (Clark and Hyne 1983). According to Clark et al. (1990a), H_2S, CO_2, H_2, CO, CH_4, and C_{2-5} gases are generated by the aquathermolysis reactions occurring between heavy oil and steam. The hydrolysis of the sulfur bridge of organosulfur compounds is the most important mechanism; the C-S bond can be cleaved to release hydrogen sulfide gas as per the following reaction (Hamedi-Shokrlu and Babadagli 2013):

$$\text{Heavy Oil} + H_2O \rightarrow CO + H_2S + \text{Lighter Organic Compounds} \quad (1)$$

The produced CO will react with water, transferring hydrogen from water to oil via the following water-gas-shift-reaction (Hamedi-Shokrlu and Babadagli 2014a):

$$CO + H_2O \Leftrightarrow CO_2 + H_2 \quad (2)$$

The produced hydrogen can attack the unstable and unsaturated molecules, which is the so-called hydrogenation effect, further improving the quality of heavy oil (Fan et al. 2002). The *in-situ* production of CO_2 is also helpful since CO_2's dissolution in crude oil can cause volume expansion and further reduce heavy oil viscosity (Wu and Carrol 2011).

Many researches have proved that transition metals can be used to catalyze aquathermolysis. To our knowledge, Clark et al. (1990b) first reported that a higher viscosity reduction can be achieved by introducing a series of transition metal ionic solution to oil sand samples. Similar work has been done by Fan et al. (2002) to prove the catalytic effect of metal species, which can be naturally present in the oil reservoirs. Hamedi-Shokrlu and Babadagli (2013, 2014ab) also investigated the catalytic effect of metal particles and the associated kinetics during aquathermolysis reactions comprehensively. Yi et al. (2017) focused on studying the performance of nickel nanoparticle in CSS reactions. The optimum nickel nanoparticle concentration, the effect of nickel nanoparticle penetration depth, and the effect of temperature were investigated in detail in their study. It was observed that using nickel nanoparticles in CSS process can effectively promote the aquathermolysis reactions and give a higher recovery factor in CSS. However, two issues related to the use of nickel nanoparticle need to be tackled: (1) Nickel is a kind of poisonous metal; exposure to high level of nickel may cause severe health problems to human (e.g., lung cancers and nasal sinus). (2) From an economic point of view, nickel nanoparticle is an expensive material, and hence utilizing this kind of metal particle will

definitely raise the cost associated with the thermal recovery of heavy oil. Thus, the catalytic effect of other metals should be explored in order to find a cheaper alternative.

Abdullah et al. (2015) investigated the effect of dispersed nanoparticulate iron oxide, acting as a catalyst, on upgrading heavy oil during toe-to-heel air injection (THAI) and they found that under the optimum condition, both the oil viscosity and sulfur content decreased significantly. Inspired by their research, the iron oxide nanoparticle, which is more environmentally-friendly and cost-effective than nickel nanoparticle, in CSS process was studied to see whether it can provide a similar catalytic effect on aquathermolysis reactions. Both Farooqui et al. (2015) and Yi et al. (2017) observed that an increase in the water production was always encountered when nickel nanoparticles were presented in the porous media. It was speculated that in addition to the increase in the oil phase mobility, the water-phase relative permeability may also increase. Interestingly, in this study, a higher amount of water production was also observed by the use of iron oxide nanoparticle. The GC analysis and the pressure profile were employed to better understand the possible reasons for the unusual increase in water production. Thus, the major objectives of this study are to (1) examine the catalytic effect of iron oxide nanoparticle during CSS process and compare the catalytic effect of iron oxide nanoparticle against that offered by nickel nanoparticle and to (2) reveal the possible reasons leading to the unusually high water production after introducing nano-metal particle in this CSS experiments.

3.2 Experimental

3.2.1 Materials

The properties of Mexican heavy oil sample used in the experiment are shown in **Table 3.1**. Nickel nanoparticles and iron oxide nanoparticles from Sigma Aldrich, Canada were used as the catalyst for aquathermolysis reactions. The size of the nickel nanoparticles falls between 40-70 nm while the iron oxide nanoparticles have a size smaller than 50 nm. A stainless cylinder from Swagelok, Canada with a volume of 300 ml was filled up with silica sand, which has a mesh size of 40-70, and the porosity of the sand packs was measured to be 34.4%. Two steel screens were installed at the inlet and outlet of the sand pack to prevent sand production and tubing blocking problems.

3.2.2 Experimental Setup

The schematic of the experimental setup is shown in **Figure 3.1**. A stainless cylinder was placed inside the oven to generate saturated steam. By simply opening the injection valve #1, steam was able to enter the sandpack. Both the oil collecting jar and the cylinder for collecting evolved gas were fully vacuumed prior to each production cycle. Then, valve #2 was opened to collect the produced materials including oil, water, and gas. In order to monitor the temperature/pressure changes in CSS cycles, two thermocouples were installed at the inlet and outlet of the sand pack cylinder, while one pressure transducer was installed at the outlet end of the sandpack cylinder (Yi et al. 2017).

3.2.3 Experimental Procedures

The experimental procedures for conducting the CSS experiments have been well covered in our previous paper (Yi et al. 2017); please refer to it for the detailed experimental procedures. Heavy oil sample, silica sand, and nano-metal particles (for experiments with the use of nickel or iron oxide nanoparticles) were first mixed by hand. Then, the mixture was gently introduced into the stainless cylinder, which was connected to the setup as a reactor. Based on the experience gained by conducting repeated experiments with the same setup, the steam generation time, steam injection time, and soaking time were set at 5.5 h, 40 min, and 20 min, respectively (Yi et al. 2017). Steam injection was initiated by opening valve #1. Once the steam injection was terminated, valve #1 was closed to enable steam soaking in the sand pack. After the soaking period, the sand pack was put on production by opening valve #2. Cyclic steam injection was continued until there was little oil production.

Table 3.2 shows the detailed experimental scheme employed in this study. Viscosity measurements were applied to the produced oil, while GC test was used in the produced gas samples. The GC tests were performed with the Multiple Gas #3 GC apparatus (SRI 8610C Gas Chromatograph, SRI Instruments, USA). To quantify the experimental uncertainties in the measurements of recovery factor, oil viscosity, and water production, the base cases, which did not involve the use of metal nanoparticles, were repeated three times; these base cases are labeled Exp #1, Exp #2, and Exp #3 in Table 3.2. Then, different concentrations of nickel and iron oxide nanoparticles were mixed with oil sands to compare their catalytic effect on aquathermolysis reactions.

3.3 Results and Discussion

3.3.1 Comparison of the Catalytic Effects Provided by Nickel and Iron Oxide Nanoparticles

To test the consistency and repeatability of the experimental results, three base-case experiments (Exps #1-3) were conducted prior to the experiments with nano-metal particles, and the recovery factors were 24.69%, 23.18%, and 23.70%, respectively, leading to a small standard deviation of 0.76% in the recovery factor (Yi et al. 2017). The viscosity of the three oil samples collected from cycle #1 of the three base-case experiments was also measured, and the comparative results are presented in **Figure 3.2**. We observe that the viscosity of the three oil samples from the base-case experiments was quite similar to each other, and the largest experimental error in viscosity measurement was found to be 5.46% at 25°C. This result further validates the consistency and repeatability of our experiments (Yi et al. 2017).

The tests on nickel and iron oxide nanoparticles were both started with a concentration of 0.5 wt% of the initial oil in place (IOIP). Then, based on the obtained oil recovery factor, we decide whether to increase or decrease the loading of the nano-metal particles. As for the nickel nanoparticle, the recovery factor was significantly boosted by introducing 0.5 wt% of nickel; thus another lower concentration was further tested to see if we could increase the oil recovery factor with a lower concentration. But, as for the iron oxide nanoparticle, a concentration of 0.5 wt% was not able to improve the oil recovery, which implies that this concentration might be too low or too high to increase the oil recovery performance of CSS. Thus, another two concentrations of iron oxide nanoparticle, i.e., 1 wt% (which is higher than 0.5 wt%) and 0.2 wt% (which is lower than 0.5 wt%), were further tested in this study.

Figure 3.3 compares the overall oil recovery factors obtained from Exps #3-6 (with different concentrations of nickel nanoparticles) and Exps #7-9 (with different concentrations of iron oxide nanoparticles). As seen from Figure 3.3, for the nickel case, the smallest increase in oil recovery factor was found to be 7.02% in Exp #6, which used 0.05wt% nickel nanoparticle, and such an increase is significantly beyond the experimental error obtained from Exps #1-3. Thus, we infer that an improvement in the oil recovery could be achieved with the use of nickel nanoparticles. Meanwhile, as for the iron oxide, the catalytic effect of this metal species was not as significant as that of nickel nanoparticle. The highest overall oil recovery factor achieved with the use of 0.2 wt% iron oxide nanoparticle was 27.56% in Exp #9, representing less

improvement of the oil recovery factor compared with Exp #1. Moreover, when 1.0 wt% of iron oxide nanoparticle was used, the catalytic effect of iron oxide nanoparticle was weakened, leading to a reduction in the recovery factor.

Figure 3.4 shows the detailed oil recovery factors that were measured at different cycles of CSS experiments with the use of the two nano-metal particles. It can be observed that the oil production of all the CSS experiments follows a similar trend; the highest recovery was always obtained at the first cycle and then tended to decline gradually. The use of nano-metal particles extended life of the CSS experiments, leading to more production in the later cycles. It can also be observed from Figure 3.4 that the recovery factors in the first two cycles of Exps #7-9 (where iron oxide nanoparticles were used) were much lower than that of Exps #4-6 (where nickel nanoparticles were used). Viscosity tests and GC analysis were both employed to explore the reasons leading to such differences in the recovery performance.

Figure 3.5 shows the viscosity-temperature relationships of the produced oil samples from the first cycle of the CSS experiments. The viscosity of the oil samples was measured at four temperatures of 25°C, 50°C, 60°C, and 80°C. As can be seen from **Figure 3.5a**, the experiments with the use of nano-metal particles (Exps #4-9) produced less viscous oil than the experiments without nano-metal particles (Exp #1), which indicates that the nano-metal particles indeed catalyzed the aquathermolysis reactions during the CSS process. It can also be observed from Figure 3.5 that the viscosity of the produced oil samples in cycle #1 of Exps #4-6 (with nickel nanoparticles) was much lower than that in cycle #1 of Exps #7-9 (with iron oxide nanoparticles). **Figure 3.5b** presents the viscosity-temperature relationship for the oil produced from cycles #3-6 of Exp #5 and #9. Figure 3.5b also indicates that in later cycles of the CSS process, the experiment with 0.2 wt% nickel nanoparticles produced less viscous oil than the experiment with 0.2 wt% of iron oxide nanoparticle. These above observations, to a certain extent, proved that the catalytic effect of nickel nanoparticles is better than the iron oxide nanoparticles throughout the whole CSS process, hence contributing to a higher oil recovery. However, by examining both Figure 3.5a and Figure3.4, we can also find that the reduction in the oil viscosity was not directly converted to an increase in the oil recovery factor in the first cycle. This might be due to the fact that the oil-phase mobility (oil-phase permeability divided by oil viscosity) was controlled by both oil-phase permeability and oil viscosity. In the early stages, the oil-phase mobility could

mainly be controlled by the oil-phase permeability. The initial oil saturation close to the injection port was high, leading to a high relative permeability of the oil phase. In later stages, the oil-phase mobility could be more affected by the oil-phase viscosity; after cycle #1, the oil recovery in Exps #4-6 became obviously higher than those in Exps #7-9.

Another interesting phenomenon shown in Figure 3.5a is that unlike the similar oil viscosity observed in Exps #4-6 (with nickel nanoparticle), the viscosity of the heavy oil samples in Exps #7-9 (with nickel nanoparticle) differed considerably. Exp #9, with 0.2 wt% iron oxide nanoparticles, produced the least viscous heavy oil, while Exp #8, with 1 wt% iron oxide nanoparticles, produced the most viscous heavy oil. This high oil viscosity observed in Exp #8, in turn, may be the reason for the low recovery factor.

Figure 3.6 shows the GC analysis results for the gas samples produced in the first cycle of Exps #1, #5-6, and #7-9. According to Rahimi and Gentzis (2006), the energy needed for the cleavage of C-S bond of organosulphur compounds is the lowest among all bonds in heavy oil. Thus, during aquathermolysis reactions, the amount of hydrogen sulfide generated is regarded as a good indication of the level of aquathermolysis reactions (Hamedi-Shokrlu and Babadagli 2013). It can be observed from Figure 3.6 that the amount of hydrogen sulfide generated was able to be detected in Exps #5, #6, and #9; however, its volume percentage differed among the three cases. The volume percentage of hydrogen sulfide was found to be 1.1 vol% in Exp #6, which was much higher than 0.5 vol% detected in Exp #5, and 0.28 vol% detected in Exp #9. This implies that, as for the first cycle, the upgrading effect of nickel nanoparticle with a concentration of 0.05 wt% was more significant than that with 0.2 wt% of nickel nanoparticle and 0.2 wt% of iron oxide nanoparticle, resulting in a lower oil viscosity and hence a higher recovery factor. Moreover, no hydrogen sulfide was detected in Exps #7-8, which used 0.5 wt% and 1.0 wt% iron oxide nanoparticles, respectively. There could still be some hydrogen sulfide generated in these two experiments, but the volume percentage was too low to be detected with our GC equipment.

To conclude, the ultimate oil recovery factor, produced oil viscosity, and evolved gas composition from these CSS experiments were all analyzed. The results show that compared with the use of iron oxide nanoparticles, the use of nickel nanoparticles led to a higher oil recovery factor, together with a lower produced-oil viscosity. Meanwhile, the GC results of the

produced gas sample reveal that a more dramatic aquathermolysis reaction could also be achieved with the nickel nanoparticles than with iron oxide nanoparticles. Thus, the catalytic effect of iron oxide nanoparticles is not as significant as nickel nanoparticles.

3.3.2 Effect of Nickel and Iron Oxide Nanoparticles Addition on Water Production

One interesting phenomenon was noticed when analyzing the results of all the CSS experiments. When either nickel nanoparticles or iron oxide nanoparticles were introduced into the sandpack, the water production started to pick up from the very first cycle. **Figure 3.7** shows the amount of water produced in each cycle of Exp #1 (base case #1) and Exps #4-9 (with nano-metal nanoparticles). Figure 3.7 also shows the standard deviation in the water cut for the first four cycles, which was determined on the basis of the results of the repeated base cases. The lowest water cut could always be obtained from the first cycle. With more steam injected into the sandpack, more condensed water tended to be accumulated in the vicinity of the injection port, leading to an increased water saturation as a function of time, along with increased relative permeability of water. Thus, as shown in Figure 3.7, the water production always tended to increase after the first cycle. More importantly, the amount of the produced water increased noticeably after introducing nano-metal nanoparticles, which was especially true in the first two cycles. However, the experimental error started to grow since cycle #3, leading to a less observable difference between the base experiment and the experiments with the use of nano-metal particles. Herein, we infer that the higher amount of gas produced by the aquathermolysis reactions was the major driving force leading to the significant increase in the water production in the early cycles of CSS experiments with nano-metal particles. Therefore, next we provide detailed justifications for this opinion.

As explained, the amount of evolved hydrogen sulfide can serve as a good indicator of the level of aquathermolysis reactions. Thus, we explore the possible correlation between water production and the amount of generated hydrogen sulfide, as plotted in **Figure 3.8**. Figure 3.8 shows that in the base case Exp #1, no hydrogen sulfide could be detected by GC, while, in Exp #5 (0.2 wt% nickel), Exp #6 (0.05 wt% nickel), and Exp #9 (0.2 wt% iron oxide), the volume percentage of hydrogen sulfide was detected by GC, and the amount of water production in these three cases was obviously higher than that in the base case. However, since the magnitude of water production in the three cases was very close to each other, and the differences among the

values were all within the experimental uncertainty, an exact correlation could not be determined between the amount of water produced and the volume percentage of hydrogen sulfide produced.

Figure 3.9 plots the volume percentage of evolved gas versus the cycle numbers of CSS tests. **Figure 3.9a** presents the volume percentage of hydrogen sulfide generated in cycle #1 and cycles #3-6 of Exps #1, #6 and #9. As seen in Figure 3.9a, although a certain amount of hydrogen sulfide was detected in cycle #1 of Exps #6 and #9, as the experiment proceeded, no hydrogen sulfide was detected in the later cycles, indicating that the aquathermolysis reactions became less active in the later cycles. It is also known that the formation of alkenes, which are typical cracking products under low hydrogen environment, can also help to tell the degree of aquathermolysis reactions (Mollaei and Maini 2010). Thus, in **Figure 3.9b** compares the volume percentages of alkenes produced in different cycles of the CSS process. In Exp #1, the volume percentage of produced alkenes in cycle #1 was 0.0017%. In Exp #6, the volume percentages of evolved alkenes from cycle #1 and cycles #3-6 were 0.31 vol% and 0.48 vol%, respectively. The average amount of alkenes in the four cycles (#3-6) was about 0.14 vol% per cycle, which was much lower than that in cycle #1, indicating a more active reaction in cycle #1. Moreover, in Exp #9, the total amount of evolved alkenes from cycles #3-6 was much smaller than that from cycle #1, which again indicates a more intense reaction took place in cycle #1.

Figure 3.10 plots the evolution of pressure at the outlet of the sandpack versus time during the soaking period in the first four cycles of Exp #1 (base case), Exp #6 (0.05 wt% nickel), and Exp #9 (0.2 wt% iron oxide). More specifically, **Figure 3.10a** shows the variation of pressure recorded in cycle #1 of the different tests. Figure 10a also shows that the pressure drop in cycle #1 of Exp #1 declined with a larger rate than the other two cases with the use of nano-metal particles. This phenomenon became more noticeable in cycle #2, as shown in **Figure 3.10b**. Figure 10b also shows that compared with Exp #6 and #9, the pressure at the outlet of the sandpack in Exp #1 started to decline much faster from the onset to the half way point of the soaking period. Due to the more significant pressure drop, the reservoir pressure during the whole soaking period in Exp #1 (without nano-metal particles) was always lower than that of Exp #6 and #9 (with nano-metal particles). The pressure difference between Exp #1 and Exp #6 and Exp #9 reached up to 50 psi at the end of the soaking period, which is way beyond the uncertainty of the pressure transducer (±0.8 % of full scale 1000 psi). **Figure 3.10c** shows the

variation of pressure in cycle #3 of the different tests; the trend of the pressure drop during the soaking period started to become different from this cycle. The pressure drop in cycle #1cycle #2 of Exp #1, which used to decline faster than those in Exp #6 and #9, showed the lowest decline rate in cycle #3. In cycle #4 of the CSS tests (**Figure 3.10d**), such trend became more significant and the pressure at the sandpack outlet at the end of the soaking period in Exp #1 was approximately 30 psi higher than that in Exp #9.

Reviewing both Figures 3.9 and 3.10, it can be found that in the early stages of the CSS experiments, more cracking products like hydrogen sulfide and alkenes could be detected in the CSS experiments with the use of nano-metal particles. Meanwhile, significantly slower pressure depletion was also encountered in these experiments, indicating better maintenance of the reservoir pressure due to the evolved gases. The boosted water production in the early cycles of the nanoparticle-aided CSS experiments can be attributed to the better maintenance of the reservoir pressure provided by the evolved gases, including hydrogen sulfide, alkenes, and carbon dioxide. These evolved gases worked together to maintain higher pressure of the sandpack, providing a larger driving force for the water flow and thus leading to enhanced water production. Moreover, acid gas like hydrogen sulfide and carbon dioxide could also dissolve in water; the dissolved gas could provide solution-gas drive mechanisms and help to increase the water production. Because more oil and water was withdrawn from the sandpack in the earlier cycles of CSS tests with the use of nano-metal particles, when it came to the later cycles, less fluid was present in the sandpack. This renders the maintenance of the reservoir pressure more difficult. Because of this, the pressure decline in Exps #4-9 could not be compensated by the gas production from aquathermolysis reactions. This, again, explains why the amount of water produced in the later cycles of Exps #4-9 was similar to that in Exp #1, albeit with more gas being generated in the later cycles of Exps #4-9 than in Exp #1.

3.4 Conclusions

Comparing the experimental results obtained from the CSS experiments with the use of nickel and iron oxide nanoparticles, the following conclusions can be drawn:

- Both nickel and iron oxide nanoparticle can catalyze the aquathermolysis reactions. However, the catalytic effect of nickel is stronger than iron oxide, and thus a higher oil

recovery and a lower oil viscosity can be obtained with the introduction of nickel nanoparticles;

- The water production tends to be boosted in the early stages of the CSS process after introducing nano-metal particles. A higher amount of evolved gas, including hydrogen sulfide and alkenes, was detected by GC analysis. Meanwhile, the recorded data shows that the pressure decline rate during the soaking period of the first two cycles of the CSS experiments with the use of nano-metal particle was much slower than in the base case. Thus, it is believed that the high gas production increased the reservoir pressure, hence leading to a higher water production; and
- Because more oil and water had been withdrawn from the sandpack in the earlier cycles of CSS tests with the use of nano-metal particles, when it came to the later cycles, less fluid was present in the sandpack. This renders the maintenance of the reservoir pressure more difficult. Because of this, the pressure decline could not be compensated by the gas production due to aquathermolysis reactions. This again explains why the amount of water produced in the later cycles of Exps #4-9 (with nano-metal particles) was similar to the base case in Exp #1 (without the use of nano-metal particles), albeit with more gas being generated in the later cycles of Exps #4-9 than in Exp #1.

Acknowledgements

This research was conducted under Prof. Tayfun Babadagli's NSERC Industrial Research Chair in Unconventional Oil Recovery (industrial partners are Petroleum Development Oman, Total E&P Recherche Développement, SIGNa Oilfield Canada, CNRL, SUNCOR, Touchstone Exploration, Sherritt Oil, PEMEX, Husky Energy, Saudi Aramco, Devon. and APEX Eng.) and NSERC Discovery Grant (No: RES0011227 and NSERC RGPIN 05394). We gratefully acknowledge these supports.

References

Al-Marshed, A., Hart, A., Leeke, G., Greaves, M., and Wood, J. 2015. Optimization of heavy oil upgrading using dispersed nanoparticulate iron oxide as a catalyst. *Energy Fuels*. **29** (10): 6306-16.

Banerjee, D. 2012. *Oil sands, heavy oil and bitumen: from recovery to refinery.* Pennwell Corp.

Clark, P.D., Clarke, R.A., Hyne, J.B. 1990a. Studies on the chemical reactions of heavy oils under steam stimulation conditions. *AOSTRA J. Res.* **6** (1): 29-39.

Clark, P.D., Clarke, R.A., Hyne, J.B., et al.1990b. Studies on the effect of metal species on oil sands undergoing steam treatments. *AOSTRA J. Res.* **6** (1): 53-64.

Clark, P.D., and Hyne, J.B. 1983. Steam-oil chemical reactions: mechanisms for the aquathermolysis of heavy oils. *AOSTRA J. Res.* **1** (1): 15-20.

Fan, H, Liu, Y., Zhang, L. et al. 2002. The study on composition changes of heavy oils during steam stimulation process. *Fuel* **81**: 1733-1738.

Farooqui, J., Babadagli, T., and Li, H. 2015. Improvement of the recovery factor using nano-metal particles at the late stages of cyclic steam stimulation. Paper SPE-174478-MS presented at the SPE Canada Heavy Oil Technical Conference, Calgary, Alberta, Canada, 9-11 June.

Franco, C.A., Cardona, L., Lopera, S.H., et al. 2016. Heavy oil upgrading and enhanced recovery in a continuous steam injection process assisted by nanoparticulated catalysts. Paper SPE-179699-MS presented at SPE Improved Oil Recovery Conference, Tulsa, Oklahoma, USA, 11-13 April.

Hamedi-Shokrlu, Y. and Babadagli, T. 2013. In-situ upgrading of heavy oil/bitumen during steam injection by use of metal nanoparticles: a study on in-situ catalysis and catalyst transportation. Paper SPE-146661 presented at the SPE Annual Technical Conference and Exhibition, Denver, Colorado, 30 October -2 November.

Hamedi-Shokrlu, Y. and Babadagli, T. 2014a. Viscosity reduction of heavy oil/bitumen using micro- and nano-metal particles during aqueous and non-aqueous thermal applications. *J. Petro. Sci. Eng.* **119**: 210-220.

Hamedi-Shokrlu, Y. and Babadagli, T. 2014b. Kinetics of the in-situ upgrading of heavy oil by nickel nanoparticle catalysts and its effect on cyclic-steam-stimulation recovery factor. *SPE Res. Eval. Eng.* **17** (3): 355-364.

Mollaei, A. and Maini, B. 2010. Steam flooding of naturally fractured reservoirs: basic concepts and recovery mechanisms. *J. Can. Petro. Tech.* **49** (1): 65-70.

Rahimi, P.M. and Gentzis, T. 2006. The chemistry of bitumen and heavy oil processing. In: *Practical advances in petroleum processing,* eds. C.S. Hsu and P.R. Robinson, Chap. 19, 149-179. New York City, New York: Springer New York.

Wu, Y. and Carroll, J. 2011. *Acid gas injection and related technologies*. John Wiley & Sons.

Yi, S., Babadagli, T., and Li, H.A. 2017. Use of nickel nanoparticles for promoting aquathermolysis reaction during cyclic steam stimulation. *SPE J.* In press.

Tables and Figures

Oil	API	Density at 25 °C (kg/m^3)	Saturates wt%	Aromatics wt%	Resins wt%	Asphaltenes wt%	Viscosity at 25°C (cp)
Mexican heavy oil	10.75	987.9	31.93	18.92	24.36	24.57	45590

Table 3.1 Properties of heavy oil sample used in Chapter #3.

Exp. No.	Temperature (°C)	Original oil viscosity (cp)	Injection duration (min)	Soaking duration (min)	Nickel concentration (g/g, wt%)	Ironoxide concentration (g/g, wt%)
1	220	45990	40	20	0	0
2	220	45990	40	20	0	0
3	220	45990	40	20	0	0
4	220	45990	40	20	0.50	0
5	220	45990	40	20	0.20	0
6	220	45990	40	20	0.05	0
7	220	45990	40	20	0	0.50
8	220	45990	40	20	0	1.00
9	220	45990	40	20	0	0.20

Table 3.2 Experimental schemes used in Chapter #3.

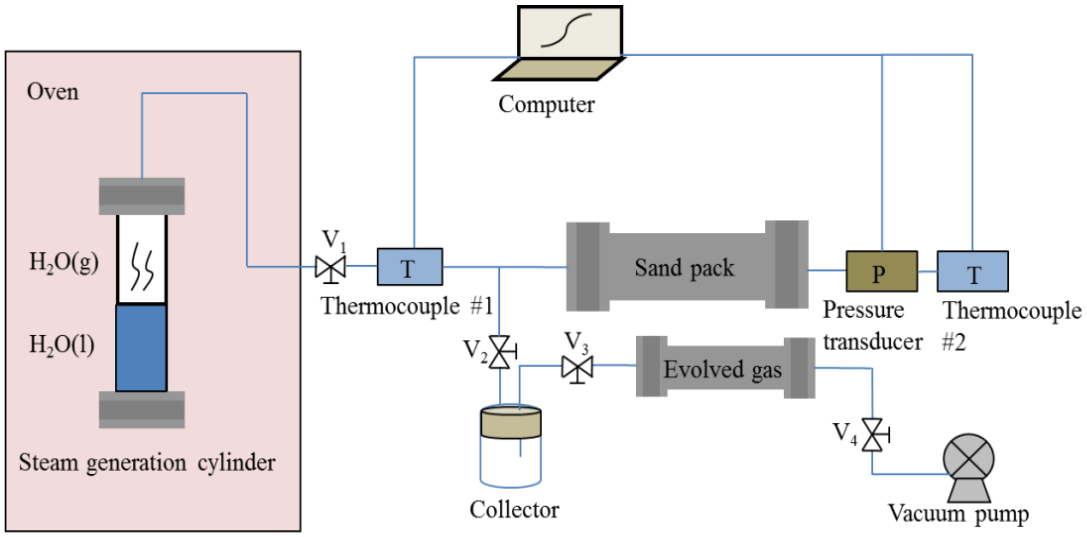

Figure 3.1 Experiment setup used for conducting the CSS experiments with the use of nano-metal particles (Yi et al. 2017).

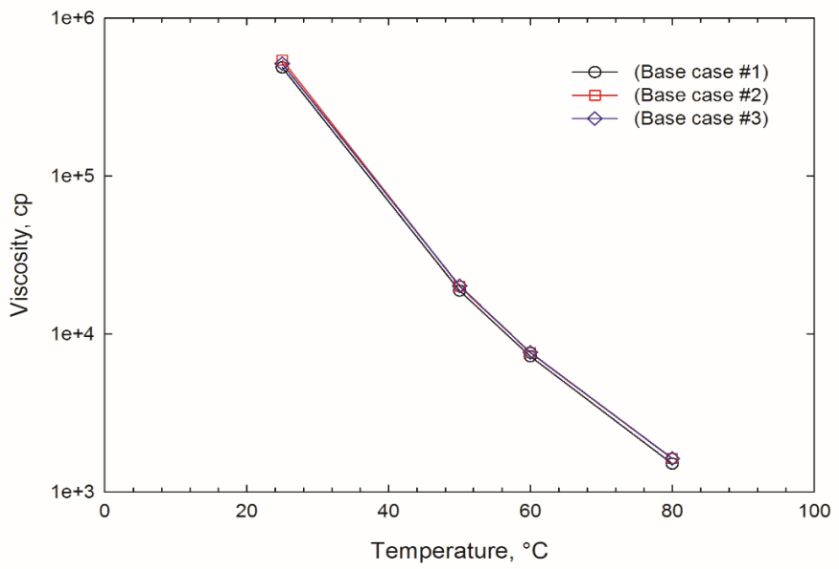

Figure 3.2 Viscosity of the oil samples that were collected at cycle #1 of CSS experiments Exps #1-3 (Yi et al. 2017).

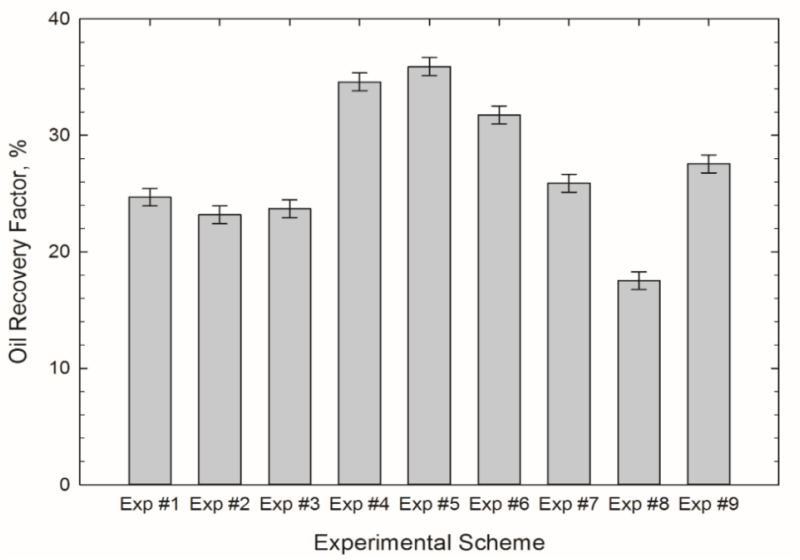

Figure 3.3 Ultimate oil recovery factors that were measured in Exp #1-3 (base cases), Exp #4-6 (experiments with nickel nanoparticles) (Yi et al. 2017), Exp #7-9 (experiments with iron oxide nanoparticles) at 220°C.

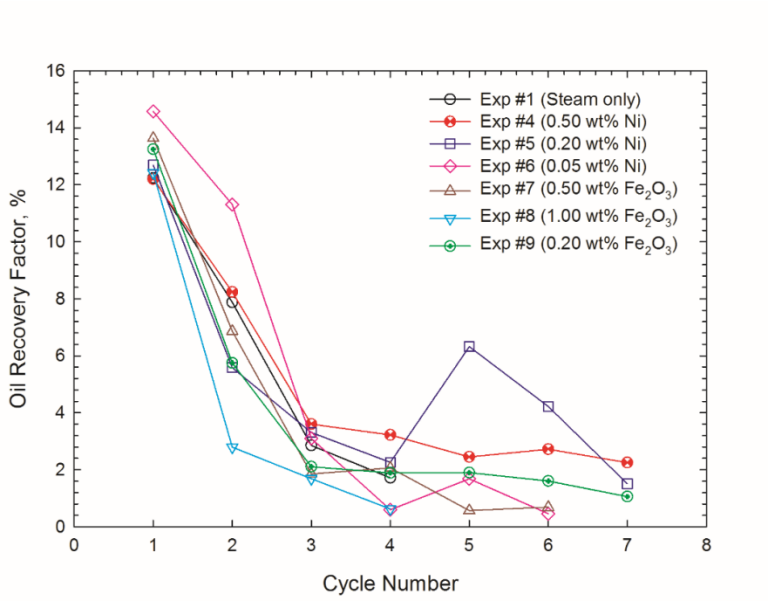

Figure 3.4 Oil recovery factors that were measured at different cycles of CSS experiments with the use of different nickel and iron oxide nanoparticle concentrations at 220°C.

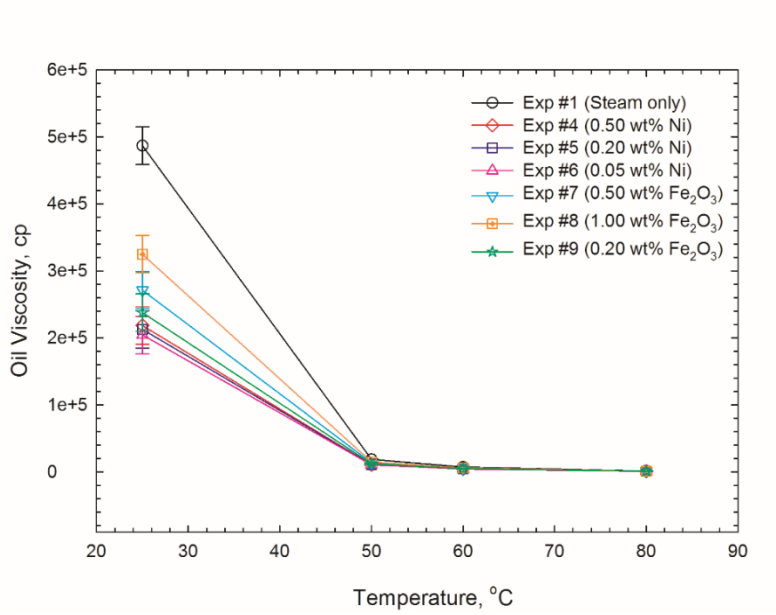

(a)

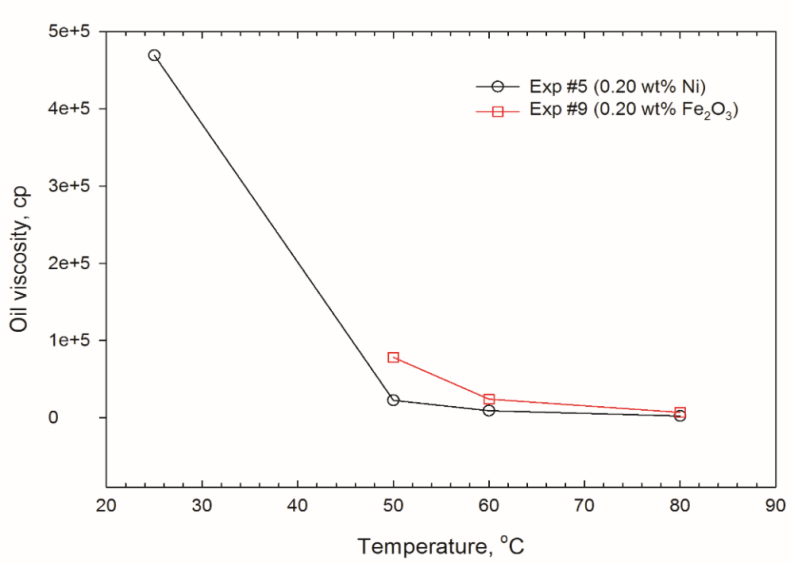

(b)

Figure 3.5 Viscosity of the oil samples that were collected at different times of the CSS experiments: a) cycle #1 of Exp #1 and Exps #4-9; b) cycle # 3-6 of Exp #5 and Exp #9.

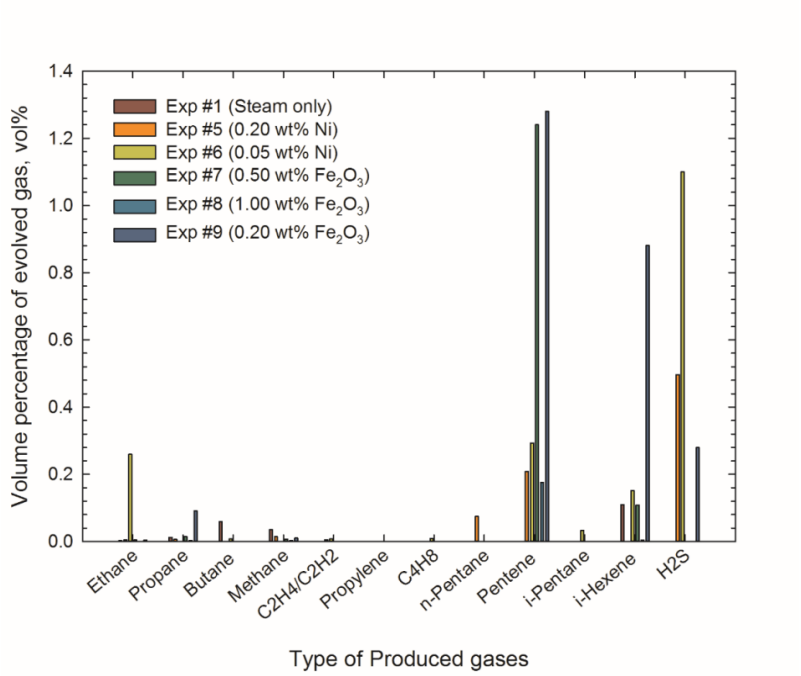

Figure 3.6 GC analysis results for the gas samples that were collected during cycle #1 of Exp #1 and Exps #5-9.

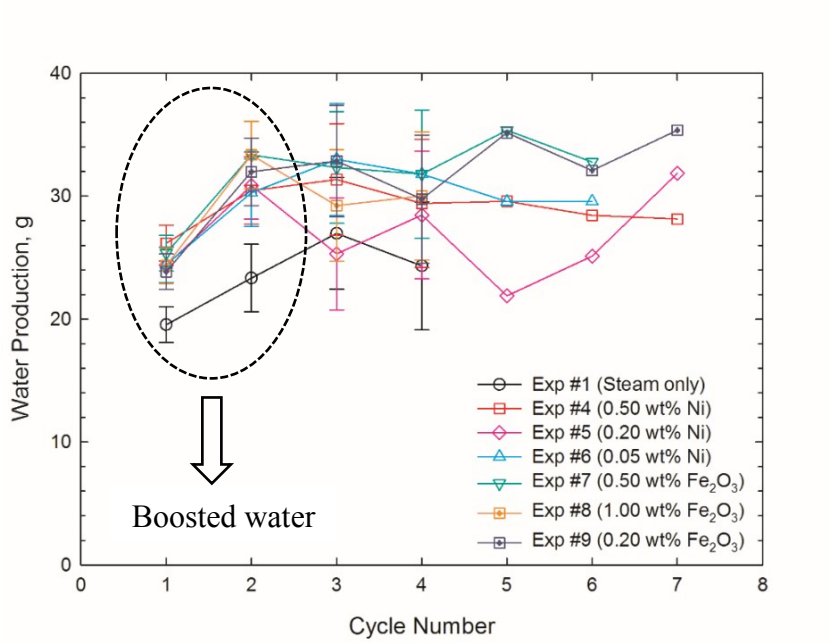

Figure 3.7 Amount of water produced at different cycles of CSS experiments.

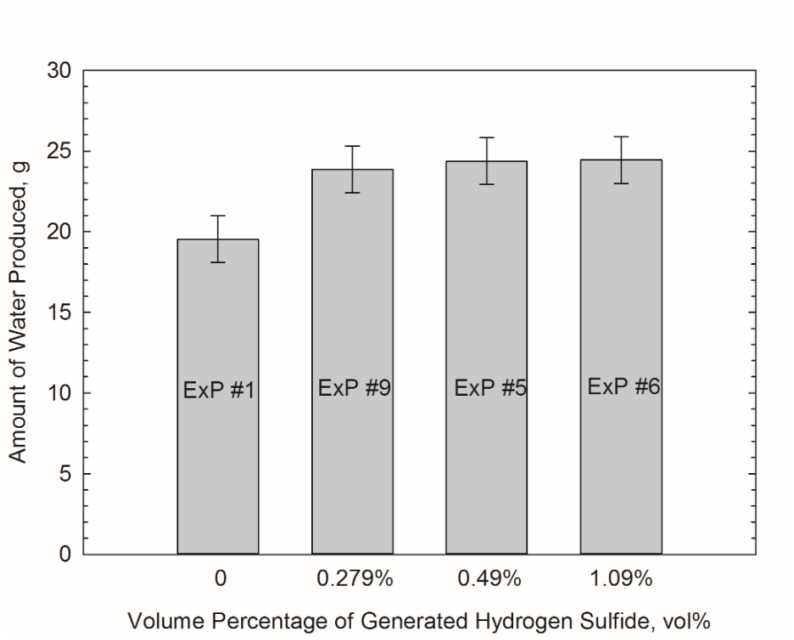

Figure 3.8 Plot of the amount of water produced versus the volume percentage of hydrogen sulfide generated in the first cycle of different CSS tests.

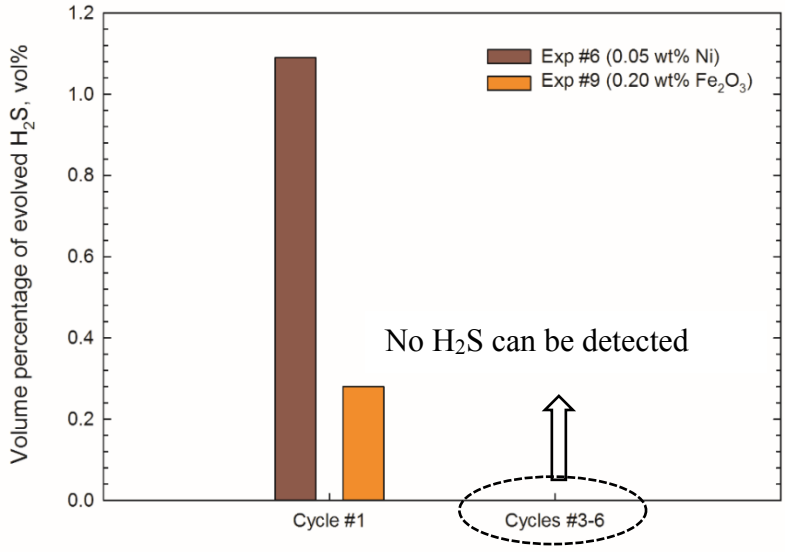

(a)

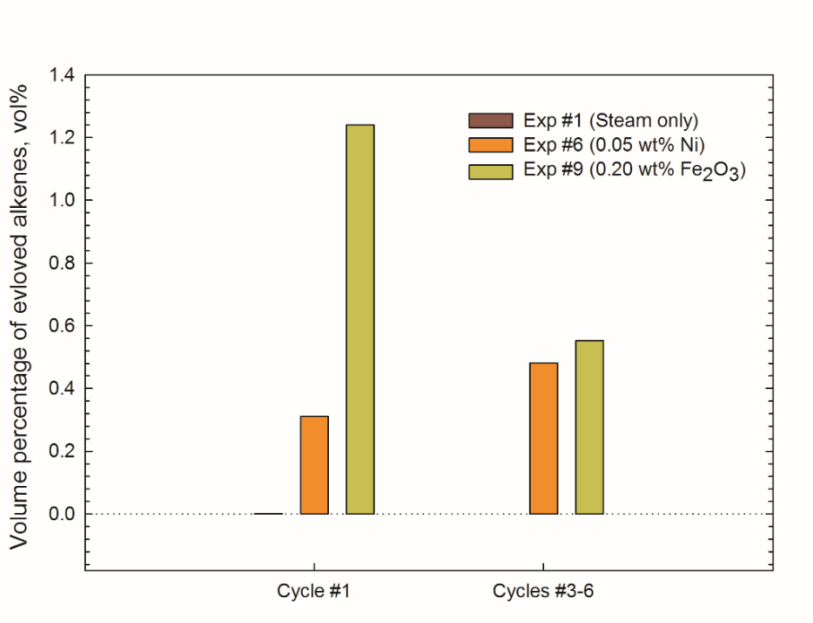

(b)

Figure 3.9 Volume percentages of evolved gas that were measured in cycle #1 and cycle #3-6 of Exp #1, #6 and #9: a) hydrogen sulfide; b) alkenes.

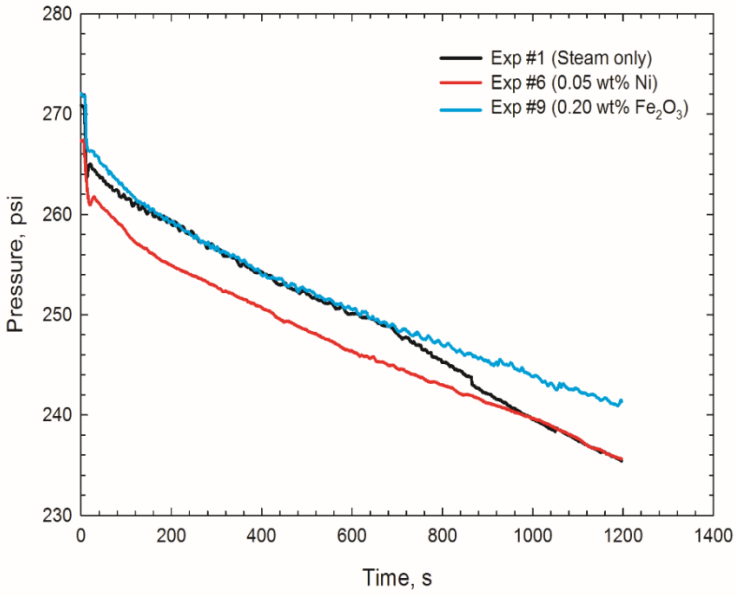

(a) Cycle #1 of Exp #1 (steam only), Exp #6 (0.05 wt% nickel), and Exp #9 (0.2 wt% iron oxide).

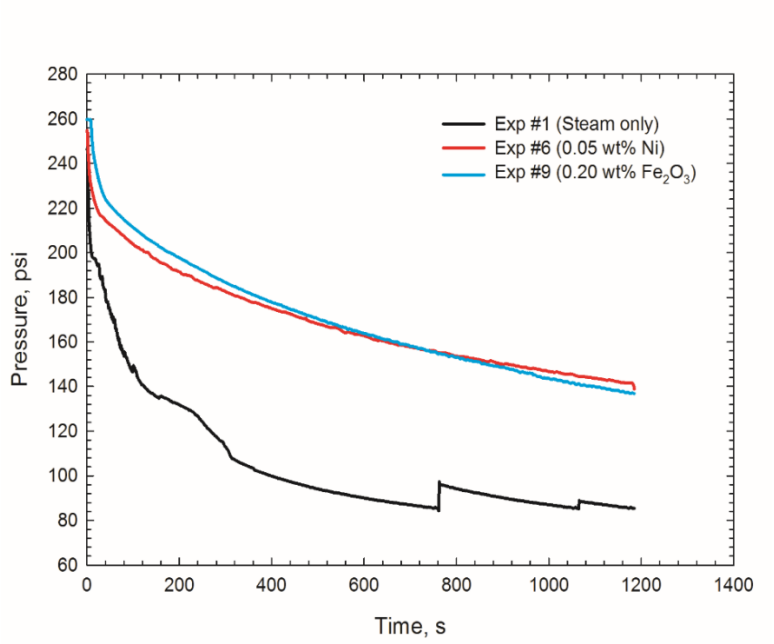

(b) Cycle #2 of Exp #1 (steam only), Exp #6 (0.05 wt% nickel), and Exp #9 (0.2 wt% iron oxide).

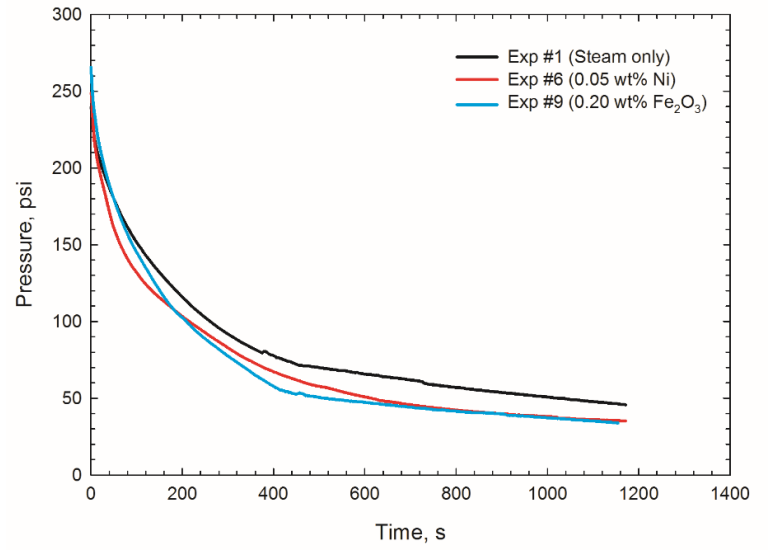

(c) Cycle #3 of Exp #1 (steam only), Exp #6 (0.05 wt% nickel), and Exp #9 (0.2 wt% iron oxide).

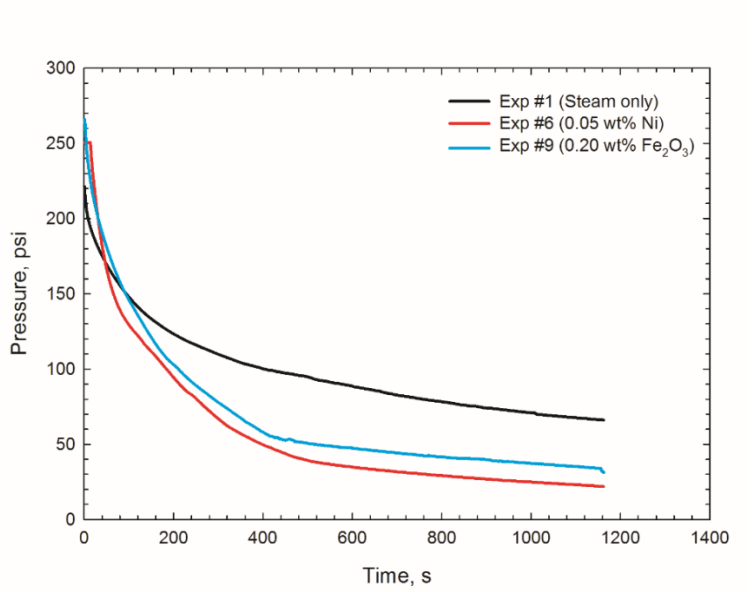

(d) Cycle #4 of Exp #1 (steam only), Exp #6 (0.05 wt% nickel), and Exp #9 (0.2 wt% iron oxide).

Figure 3.10 Variation of pressure at the outlet of the sandpack versus time during the soaking period in different cycles of the CSS tests.

CHAPTER 4 Stabilization of Nickel Nanoparticle Suspensions with the Aid of Polymer and Surfactant: Static Bottle Tests and Dynamic Micromodel Flow Tests

A version of this chapter will be submitted to *Colloids and Surfaces A, 2017.*

Abstract

Nickel nanoparticles can work as catalyst for the aquathermolysis reactions between water and heavy oil. A homogeneous and stable nickel nanoparticle suspension is needed to carry the nickel nanoparticles into deeper reservoirs. This study conducts a detailed investigation on how to achieve stabilized nickel nanoparticle suspensions with the use of surfactant and polymer. To stabilize the nickel nanoparticle suspension, Xanthan gum polymer and surfactant (SDS, CTAB or Hypermer KD-2) were introduced into the nickel nanoparticle suspension. Visual tests were then conducted to observe how the nickel nanoparticles would settle in the suspensions. Factors including polymer concentration, surfactant type, and surfactant concentration were considered in the tests. Zeta potential of the suspensions was also measured. Three nickel nanoparticle suspensions recipes were found to be most stable: #1-1.000 wt% Ni/0.350 wt% SDS/0.045 wt% Xanthan gum, #2-1.000 wt% Ni/0.350 wt%/Hypermer KD-2/0.045 wt% Xanthan gum, and #3-2.000 wt% Ni/0.500 wt% SDS/0.060 wt% Xanthan gum. Micromodel-based visualization tests were conducted on the three suspensions to reveal how the nickel nanoparticles would travel and distribute in the porous media when being injected into the porous media. Test results show that when the injection was initiated, most nickel nanoparticles were able to pass through the gaps between the sand grains and produce in the outlet of the micromodel; only a small amount of the nickel nanoparticles was attached to the grain surface. A higher nickel concentration in the suspension may lead to agglomeration of nickel nanoparticles in the porous media, while a lower concentration can mitigate this agglomeration. Moreover, clusters tended to form when the nickel nanoparticle suspension carried an electrical charge opposite to that of the porous media. Follow-up water flooding was initiated after the nanofluid injection. Water flooding was found to be unable flush away the nanoparticles that were remaining in the micromodel.

Keywords: Nickel Nanofluid Stabilization, Surfactant/Polymer, Nickel Nanoparticle Transportation, Nickel Nanoparticle Distribution, Nickel nanoparticle Concentration, Surface Charge

4.1 Introduction

Nano technology has found applications in many industries such as electronics, medical, materials, and petroleum (Kim et al. 2015). It has been reported by Kong and Ohadi (2010) that nano technology is capable of bringing revolutionary changes in the fields of oil exploration,

drilling, production, enhanced oil recovery (EOR), etc. For example, a more detailed and accurate description of the reservoir can be provided with the use of nanosensors in the reservoir, and the use of nanomembranes can help to effectively remove impurities from oil and gas streams (Kong and Ohadi 2010). Moreover, the oil recovery could be improved by injecting nanoparticles into the porous media along with the *in-situ* upgrading of heavy oil and bitumen. As reported by Clark et al. (1990), transition metal species can act as catalyst for aquathermolysis reactions (chemical reactions between oil and steam that release hydrocarbon gases, hydrogen sulfide, carbon dioxide and hydrogen, and further reduce the heavy oil viscosity) and *in-situ* upgrading heavy oil.

Later, many researchers started to study the catalytic effect that metal species have on the aquathermolysis reactions. A viscosity reduction along with a decrease in the mean molecular weight of the extra-heavy oil was observed in the experiments conducted by Wei et al. (2007) with the use of nickel nanoparticle. By conducting experiments with trimetallic nanocatalysts, enhanced oil recovery was obtained by Hashemi et al. (2013). Ragab and Hannora (2015) injected silica nanofluid into sandstone core and found that the finer the nano particle, the higher the oil recovery achieved.

Built upon these research achievements, Yi et al. (2017) conducted an experimental study on the use of nickel nanoparticles for promoting aquathermolysis reactions during cyclic steam stimulation. Under the experimental conditions, the optimum nickel nanoparticle concentration was found to be 0.2 wt%; but, it should be noted that these experiments were conducted with nanoparticles premixed into the sandpack. To better simulate the field condition, the nickel nanoparticle should be introduced into the reservoir in the form of nanofluid that is stable under reservoir conditions. However, due to its high surface energy, nanoparticles have a high tendency of agglomeration, making their suspension in a base fluid challenging (Li et al. 2007). Therefore, to achieve a better recovery performance, it is of critical importance to ensure that the nanoparticle suspension is stable and can carry the nanoparticles into deeper locations of the reservoir.

The London-van der Waals attractive force and the electrostatic repulsion between two charged particles are the two major forces affecting the stability of nanofluid (Williams et al. 2006). Certain surface treatment on the nanoparticles is a commonly applied technique to

achieve a better stabilization effect of nanofluids (Williams et al. 2006). Particle surface charge can be created by adding acid or charged surfactants into the suspension. For example, Li et al. (2007) tested the performance of three surfactants, TX-10, CTAB, and SDBS, in stabilizing copper nanoparticle suspensions, and studied the influences of surfactant type, surfactant concentration, and pH on the suspension stabilization. Hwang et al. (2007) tested the use of SDS and oleic acid to stabilize nanofluids, finding that surfactants helped to create stable nanofluids by increasing the magnitude of the zeta potential. Xue and Sethi (2012) achieved the stabilization of a highly concentrated iron nanofluid using a mixture of guar gum and Xanthan gum polymer. Kim et al. (2015) introduced a polymeric surfactant Hypermer KD2 to prevent aggregation of nickel nanoparticles before synthesis. Inspired by the these studies, cationic surfactant CTAB, anionic surfactant SDS, and polymeric surfactant Hypermer KD2 were introduced into nickel nanofluid separately or in mixture form together with xanthan gum polymer to stabilize the nickel nanofluid.

When nanofluid is injected into the porous media, a deeper transportation, and a better attachment of particle to oil/water interface and sand grains are both important. The transportation of nanoparticle flow in porous and fractured media has been studied by Alaskar et al. (2012). They demonstrated that the particle size, size distribution, particle shape, and particle surface charge are influential parameters governing the transport of nanoparticles through porous media. It was concluded that the particles with an opposite surface charge with the porous media tended to become trapped due to the affinity to the porous matrix, and surface modification with surfactant could improve its transport in the pore spaces. However, according to the investigation by Hamedi-Shokrlu and Babadagli (2014), in order to successfully let the nickel nanoparticles migrate to oil-water interfaces, the modification of the surface charge of oil phase by surfactant (having a surface charge opposite to that of the nanofluid) is required. In other words, the surface charge of the oil phase must be opposite to the charge of the nickel nanoparticles so that a better attachment of nickel nanoparticles can be achieved. However, in their study, a very low nickel nanoparticle concentration (0.050 wt%) was employed. In our study, the concentration of nickel nanoparticle was as high as 1.000 wt% and 2.000 wt%. Thus, to explore how the nickel nanoparticle would travel in the porous media with such a high concentration, dynamic micromodel experiments were also carried out in this study.

To conclude, three surfactants (including CTAB, SDS and Hypermer KD-2) along with Xanthan gum polymer were tested in this study to determine the polymer/surfactant recipe yielding the most stable nickel nanoparticle suspensions. In addition, micromodel tests were conducted to investigate the effect of nickel nanoparticle concentration and surface charge on the transport of nickel nanoparticles in the porous media.

4.2 Experimental

4.2.1 Materials

The diameter of the nickel nanoparticles (Sigma Aldrich, Canada) used in this study was in the range of 40-70 nm. Silica sand with the US mesh size of 40-70 was mixed with the mineral oil to make the micromodel. The mineral oil had a viscosity of 15000 cp at 25°C. Three types of surfactants were considered in this study, i.e., anionic surfactant sodium dodecyl sulfate (SDS) ($NaC_{12}H_{25}SO_4$), cationic surfactant cetyltrimethylammonium bromide (CTAB) ($C_{19}H_{42}BrN$), and polyoxyalkalene amine derivative (Hypermer KD-2), which is a polymeric surfactant. The anionic polymer xanthan gum ($C_{35}H_{49}O_{29}$) was also tested in terms of its performance in stabilizing the nickel nanoparticle suspension.

4.2.2 Experimental Procedures

This section describes the procedures for conducting the static stability test on the nickel nanoparticle suspensions, and the procedures for conducting the dynamic micromodel flow test. **Figure 4.1** shows the schematic diagram of the experimental setup used for the dynamic micromodel flow test. In the beginning of the stability test, the nickel nanoparticle was added to the deionized water, resulting in nickel nanoparticle suspensions with weight concentrations of 1.000 wt% or 2.000 wt%. Then, ultrasonication with a power of 200 W was applied to the suspension for 40 min to disperse nickel nanoparticles. Next, surfactant or the mixture of surfactant and Xanthan gum polymer was added into the nickel nanoparticle suspension, followed by a 40 min stirring of the suspension. Afterwards, visual tests were conducted to observe the sedimentation process of the nickel nanoparticles in the suspension. We also measured the zeta potential of the most stable suspension solution. The detailed experimental scenarios are shown in **Table 4.1**. Based on the static stability tests, the polymer/surfactant recipe yielding the most stable nanoparticle suspensions were then determined.

The dynamic micromodel flow tests were conducted after the stability test. Silica sands were first mixed with the mineral oil dyed with fluorescent. Then, the silica sands mixed with mineral oil were spread on one glass sheet and subsequently covered by another sheet to make the micromodel. A syringe pump was used to inject the nickel nanoparticle suspension into the micromodel, and the camera attached to the microscope was employed to monitor the migration of the nickel nanoparticles in the micromodel.

4.3 Results and Discussion

4.3.1 Static Stability Tests of Nickel Nanoparticle Suspensions

Figure 4.2 shows the images of water mixed with the nickel nanoparticles before and after ultrasonication. When mixed with deionized water, the nickel nanoparticles can aggregate due to the strong van der Waals interactions, as depicted in **Figure 4.2(a)**. However, as can be observed in **Figure 4.2(b)**, when being treated by ultrasonication, the agglomeration could be disturbed and the nickel nanoparticles could disperse in the deionized water homogeneously, forming nickel nanoparticle suspension. However, when the ultrasonication was terminated, these nickel nanoparticles will aggregate and precipitate again. **Figure 4.3** shows the images captured in Exp. #1 at different times after the ultrasonication was terminated. As shown in Figure 4.3, a clear interface appeared 2 min after the sample preparation; after 8 min, the majority of the nickel nanoparticles precipitated again.

Previously, two approaches were used to enhance the stability of the nanoparticle suspension: (1) To enhance the electric repulsion force among nickel nanoparticles by using surfactant; (2) to increase the viscosity of the base fluid to decrease the settling velocity of the particles (Hamedi-Shokrlu and Babadagli 2014). In Exp #2, cationic surfactant CTAB was added to enhance the stability of the nickel nanoparticle suspension. **Figure 4.4** shows the images of the nickel nanoparticle suspension (prepared with 1.000 wt% CTAB surfactant) captured at different times after ultra-sonication. As observed in Figure 4, the nickel suspension prepared with 1.0 wt% CTAB exhibited poor stability. Moreover, we conducted the stability test on suspensions prepared with other CTAB concentrations and observed the same phenomenon as shown in Figure 4.4. Based on the observation from Li et al. (2007), by introducing the CTAB, the nanoparticles tend to form agglomerated structure when pH is lower than 7, while a good dispersion can result when pH is in the range of 9-10. Therefore, the neutral pH level (pH=7) of

the tested suspension in this study may be the reason leading to the instability of the nickel nanoparticle suspensions. Subsequently, we tested the stability of the suspension prepared with Xanthan gum polymer and CTAB surfactant in Exp #3. **Figure 4.5** shows the images of the nickel nanoparticle suspension (prepared with 1.000 wt% CTAB and 0.030 wt% Xanthan gum polymer) captured at different times after ultrasonication. As expected, a rapid agglomeration of nickel was observed in this test due to the opposite surface charge between CTAB and Xanthan gum polymer.

Figure 4.6 shows the images of the nickel nanoparticle suspension (prepared with 0.350 wt% SDS) captured at different times after ultrasonication. Compared with the suspension prepared with CTAB, the nickel nanoparticle suspension prepared with SDS was more stable and no obvious precipitation was observed after 8 min. Thereof, SDS can be used to enhance the stability of nickel nanoparticle suspension; however, after 20 min, it started to aggregate and the aggregation became more serious after 40 min.

Xanthan gum polymer was then introduced into the nickel nanoparticle suspension with 0.350 wt% SDS to improve the stability of the suspension. The Xanthan gum polymer dissolved in water increased the stability of the nickel nanoparticle suspension by increasing its viscosity. However, the chance of formation clogging increases as viscosity of the fluid increases (Hamedi-Shokrlu and Babadagli 2014). Therefore, when preparing the nickel nanoparticle suspension, the viscosity of suspension is the key parameter to consider. To obtain a proper suspension viscosity, in Exp #5, we initially prepared the suspension with 0.030 wt% of Xanthan gum polymer, with a viscosity of 1.7 cp at 25^{o}C. However, as can be observed in Figure 6, the suspension aggregated within 40 min due to the high nickel concentration. Thus, we increased the polymer concentration to 0.045 wt% with different SDS added. **Figure 4.7** shows the images of the nickel nanoparticle suspension prepared with 0.045 wt% Xanthan gum polymer and 0.350 wt% SDS. As shown in Figure 7, no aggregation is observed in the suspension even after 60 min; the zeta potential of this suspension -52 mv, confirming good stability. The reason for using surfactant together with polymer to prepare the suspension is not only because the surfactant can increase the surface charge of the particles, but it can also decrease interfacial tension between oil and water.

Another surfactant is Hypermer KD-2, a liquefied polymeric surfactant with a viscosity of 135 cp at 25°C. Based on the observation from Kim et al. (2005), Hypermer KD-2 can stabilize nickel nanoparticle suspension for over 1 week. However, in Exps #8-10, even when the concentration of Hypermer KD-2 was increased from 0.500 wt% to 2.000 wt%, the stabilization of the suspension experienced little change, probably caused by the high concentration of nickel nanoparticles. In Exp #11, 0.045 wt% of Xanthan gum polymer together with 0.350 wt% of Hypermer KD-2 surfactant was added into the suspension. **Figure 4.8** shows the images captured during Exp #11 after ultrasonication. As seen from Figure 8, there was no aggregation observed in the suspension even after 60 min; therefore, this suspension exhibited a good stability. The zeta potential of this suspension was measured to be -55 mv, validating good stability of this nickel nanoparticle suspension.

To summarize, the surfactant alone, i.e. CTAB, SDS, Hypermer KD-2, could not greatly enhance the stability of the nickel nanoparticle suspension. However, when being used together with Xanthan gum polymer, it could increase the stability of the suspension. We found that 0.045 wt% Xanthan gum polymer and 0.350 wt% of surfactant SDS or 0.045 wt% Xanthan gum polymer and 0.350 wt% Hypermer KD-2 could stabilize the suspension for as long as 60 min. However, if the concentration of nickel nanoparticle increased to 2.000 wt%, a higher concentration of surfactant and polymer (i.e. 0.060 wt% Xanthan gum polymer and 0.500 wt% SDS) was required to stabilize the suspension.

4.3.2 Dynamic Micromodel Flow Test

After determining the polymer/surfactant recipes giving the most stable nickel nanoparticle suspensions, dynamic micromodel flow tests were conducted using these suspensions to investigate the migration of nanoparticles in the micromodel. An initial injection rate of 0.05 mL/min was first applied to study the transport of the injected particles in the porous media. Exp #2.1 used the suspension prepared with 2.000 wt% nickel nanoparticle, 0.500 wt% SDS, and 0.060 wt% Xanthan gum polymer. **Figure 4.9** shows the images at the injection port before and after the nanofluid injection. In **Figure 4.9a)**, the channels at the injection port before the suspension injection can be clearly observed. As depicted in **Figure 4.9(b)**, after injecting the suspension (2.000 wt% nickel nanoparticles, 0.500 wt% SDS, and 0.060 wt% Xanthan gum polymer) into the micromodel, both the small and large pores were blocked, which was possibly

caused by the high concentration of nickel nanoparticles in the suspension. The nickel nanoparticle with such a high concentration may be easily adsorbed on the surface of the silica sands due to the strong surface/particle interactions.

The suspension injection was stopped right before the breakthrough of the suspension. Then, water flooding was conducted to investigate the effect of injected water on the distribution of nanoparticles in the pore configurations. **Figure 4.10** shows the distributions of the nickel nanoparticles in the pore configurations before and after the water flooding. It can be seen that distribution of the nanoparticles was almost unchanged when the injection rate was low (i.e., 0.05 mL/min). As shown in **Figure 4.10(b)**, the distribution of these nanoparticles after water flooding was identical to the water flooding before. Consequently, we further investigated the sensitivity of the distribution to the injection rate by increasing the injection rate of water. After increasing the injection rate to 0.5 mL/min, the distribution of the nanoparticles remained unchanged in the micromodel. This may be because of the following two reasons: (1) The low injection rate and as a result the viscous force was not able to remove the precipitated nanoparticles and (2) because the injected water might have flown through the pores that were unblocked by the nickel nanoparticles. **Figure 4.11** presents the distribution of the particles at other locations in the micromodel. As depicted in Figure 4.11, the nanoparticles were mostly present in the injection end while few nanoparticles were present in other areas. These visual observations indicate that only a small amount of nickel nanoparticles tended to be attached to the sand surface; most the particles had been transported into the production end.

In Exp. #2.2, nickel nanofluid comprising of 1.000 wt% nickel, 0.350 wt% SDS, and 0.045 wt% Xanthan polymer was injected into the porous media. Similarly, most of the particles tended to flow towards the production end during the injection period. Moreover, it was observed that the distribution and attachment of the nanoparticles were also not influenced by water flooding. **Figure 4.12** shows the images taken after water flooding. As indicated by Figure 4.12(a)-(c), less agglomeration was observed near the injection port for the suspension with lower nickel concentration. **Figure 4.13** presents the distribution of the nickel nanoparticles in micromodel after water flooding in Exp #2.3 (1.000 wt% nickel suspension, 0.350 wt% Hypermer-KD 2, and 0.045 wt% Xanthan gum polymer). It can be seen from Figure 4.13 that the nickel nanoparticles,

either near the injection port or around the production point, appeared to be uniformly attached on the surface of sand grains.

Hamedi-Shouklu and Babadagli (2014) conducted micromodel experiments by injecting CTAB solution into a micromodel first, followed by injecting nickel nanoparticle suspension with Xanthan polymer. They proposed that one slug of CTAB surfactant should be injected to alter the surface charge of the silica sands, enabling the nickel nanoparticle to be moved more easily to the sand surface. As observed from Exp #2.2 and #2.3, when nickel nanoparticles made contact with the silica sands, the negatively charged nickel nanoparticles could get adsorbed on the sand surface. In Exp #2.4, CTAB was first injected to alter the surface charges of the sand grains, followed by injection of nickel nanoparticle suspension. **Figure 4.14** shows the images taken at different locations of the micromodel in Exp #2.4 after water flooding. It can be seen from Figure 4.14 that after the surface charge of sands was altered from negative to positive, large clusters of nickel nanoparticle could form and become trapped on the sand surface.

To summarize, as observed from the micromodel experiments, nanofluid with a lower nickel concentration could help to increase the injectivity of the nanoparticles. If the injected nanofluid had a surface charge opposite to that of the porous media, clusters could be formed more easily on the sand surface, hampering the migration of the nanoparticles into the deeper reservoir. In the field application, a suitable concentration of nickel nanoparticles should be selected, and the charges of both the injected suspension and the pore surface should be considered in order to achieve a desirable placement of the nanoparticles.

4.4 Conclusions

In this study, stability tests were conducted on nickel nanoparticle suspensions that were prepared with polymer and surfactant additives, followed by the dynamic flow test to investigate the migration of such nanoparticles in the micromodel. The detailed conclusions can be drawn as below:

(1) The individual surfactant, i.e. CTAB, SDS, and Hypermer KD-2, cannot greatly stabilize the nickel nanoparticle suspension;

(2) After introducing a certain amount of Xanthan polymer into the system, the stability of such nickel nanoparticle suspension was improved. The recipes determined that are considered to significantly enhance the stability of the suspension are: 1.000 wt% Ni + 0.350 wt% SDS +

0.045 wt% Xanthan polymer, 1.000 wt% Ni + 0.350 wt% Hypermer KD-2 + 0.045 wt% Xanthan polymer, and 2.000 wt% Ni + 0.500 wt% Ni + 0.060 wt% Xanthan polymer;

(3) When suspension comprising of high concentration, i.e. 2.000 wt% of nickel nanoparticle is injected into the micromodel, the nickel nanoparticles tends to agglomerate severely and then block the channels near the injection port;

(4) A smaller amount of the nickel nanoparticles is attached to the surface of the sand grains when nanoparticle has the same surface charge with the silica sand; and

(5) When the silica sands were first treated with CTAB surfactant, alternating its surface charge from negative to positive, larger clusters will form and the particles may trap in the porous media.

Acknowledgements

This research was conducted under Prof. Tayfun Babadagli's NSERC Industrial Research Chair in Unconventional Oil Recovery (industrial partners are Petroleum Development Oman, Total E&P Recherche Développement, SIGNa Oilfield Canada, CNRL, SUNCOR, Touchstone Exploration, Sherritt Oil, PEMEX, Husky Energy, Saudi Aramco, Devon. and APEX Eng.) and NSERC Discovery Grant (No: RES0011227 and NSERC RGPIN 05394). We gratefully acknowledge these supports.

References

Alaskar, M., Ames, M., Connor S., Liu, C., Cui, Y., Li, K. and Horne, R. Nanoparticle and microparticle flow in porous and fractured media – an experimental study. 2012. *SPE J.* **17** (04): 1-160.

Clark, P.D., Clarke, R.A., and Hyne, J.B. 1990. Studies on the effect of metal species on oil sands undergoing steam treatments. *AOSTRA J. Res.* **6** (1): 53-64.

Hamedi Shokrlu, Y. and Babadagli, T. 2014. Stabilization of nanometal catalysts and their interaction with oleic phase in porous media during enhanced oil recovery. *Ind. Eng. Chem. Res.* **53** (20): 8664-8475.

Hashemi, R., Nassar, N.N. and Pereira Almao, P., 2013. Enhanced heavy oil recovery by in situ prepared ultradispersed multimetallic nanoparticles: a study of hot fluid flooding for athabasca bitumen recovery. *Energy Fuels.* **27** (4): 2194-2201.

Hwang, Y., Lee, J.K., Lee, J.K., et al. 2008. Production and dispersion stability of nanoparticles in nanofluids. *Powder Tech*. **186** (2): 145-153.

Kim, C.K., Lee, G.J., Lee, M.K. et al. 2015. A study on dispersion stability of nickel nanoparticles synthesized by wire explosion in liquid media. *Arch. Metal. Mater.* **60** (2): 1379-1382.

Kong, X. and Ohadi, M. 2010. Applications of micro and nano technologies in the oil and gas industry-overview of the recent progress. Paper SPE-138241-MS Presented at SPE International Petroleum Exhibition and Conference, Abu Dhabi, Dubai, 1-4 November.

Li, X., Zhu, D. and Wang, X. 2007. Evaluation on dispersion behavior of the aqueous copper nano-suspensions. *J. Colloid Interf. Sci.* **310** (2): 456-463.

Ragab, A.M.S. and Hannora, A.E. 2015. An experimental investigation of silica nano particles for enhanced oil recovery applications. SPE-175829-MS Presented at SPE North Africa Technical Conference and Exhibition, Cairo, Egypt, 14-16 September.

Wei, L., Zhu, J.H. and Qi, J.H. 2007. Application of nano-nickel catalyst in the viscosity reduction of liaohe extra-heavy oil by aqua-thermolysis. *J. Fuel Chem. Tech.* **35** (2): 176-180.

Williams, W.C., Bang, I.C., Forrest, E., et al. 2006. Preparation and characterization of various nanofluids. Proc: *NSTI Nanotechnology Conference and Trade Show*. (2): 408-411.

Xue, D. and Sethi, R. 2012. Viscoelastic gels of guar and xanthan gum mixtures provide long-term stabilization of iron micro-and nanoparticles. *J. Nanopart. Res*. **14** (11): 1239.

Yi, S., Babadagli, T., Li, H.A. 2017. Use of nickel nanoparticles for promoting aquathermolysis reaction during cyclic steam stimulation. *SPE J.* In press.

Tables and Figures

Exp. #	Nickel concentration (wt %)	Surfactant type	Surfactant concentration (wt %)	Polymer concentration (wt %)
1	1	none	0	0
2	1	CTAB	1.00	0
3	1	CTAB	1.00	0.030
4	1	SDS	0.35	0
5	1	SDS	0.50	0
6	1	SDS	0.50	0.030
7	1	SDS	0.50	0.045
8	1	SDS	0.35	0.045
9	1	KD2	0.35	0
10	1	KD2	1.00	0
11	1	KD2	2.00	0
12	1	KD2	0.35	0.045
13	2	SDS	0.50	0.060

Table 4.1 Experimental schemes employed in the static stability tests conducted on the nanoparticle suspensions.

Exp. #	Nickel concentration (wt %)	Surfactant type	Surfactant concentration (wt %)	Polymer concentration (wt%)	Comment
2.1	2	SDS	0.500	0.060	Directly inject the nanoparticle suspension
2.2	1	SDS	0.350	0.045	Directly inject the nanoparticle suspension
2.3	1	KD-2	0.350	0.045	Directly inject the nanoparticle suspension
2.4	1	CTAB	1.000	0.045	Inject CTAB first, followed by injection of nickel nanoparticle suspension.

Table 4.2 Experimental schemes employed in the dynamic flow tests.

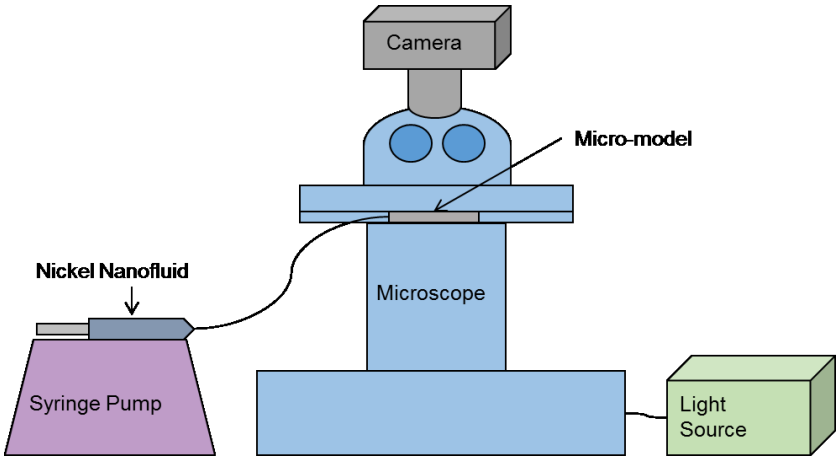

Figure 4.1 Schematic of the experimental setup used for conducting the dynamic flow test.

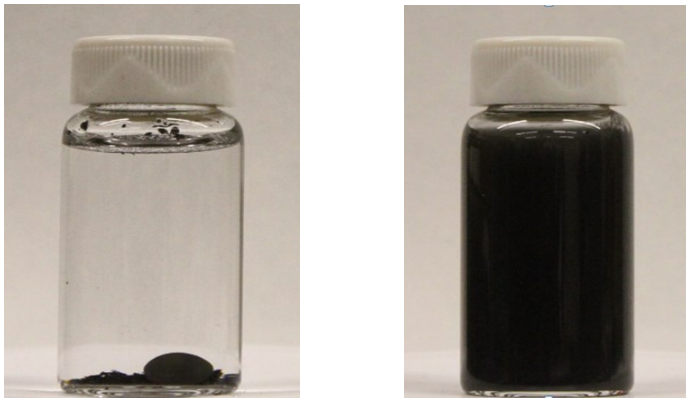

(a) **(b)**

Figure 4.2 Nickel nanoparticle in deionized water: (a) before ultrasonication; (b) after ultrasonication.

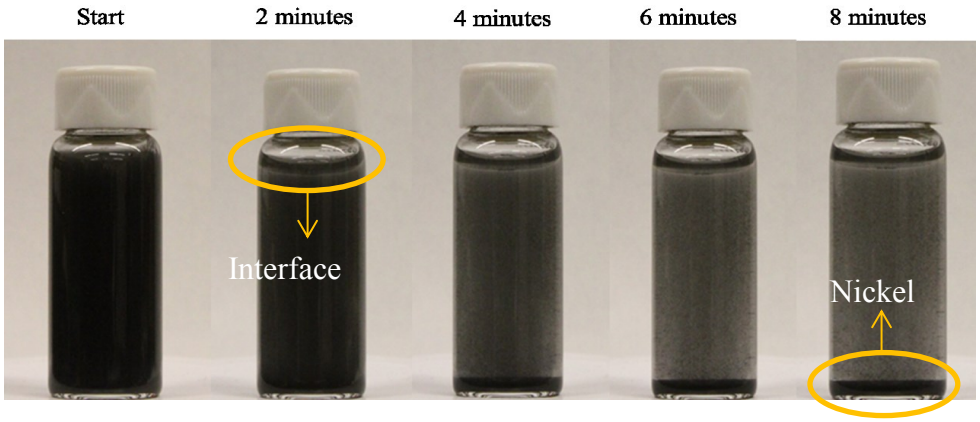

Figure 4.3 Images of the nickel nanoparticle suspension (prepared without surfactant or polymer) captured at different times after ultrasonication.

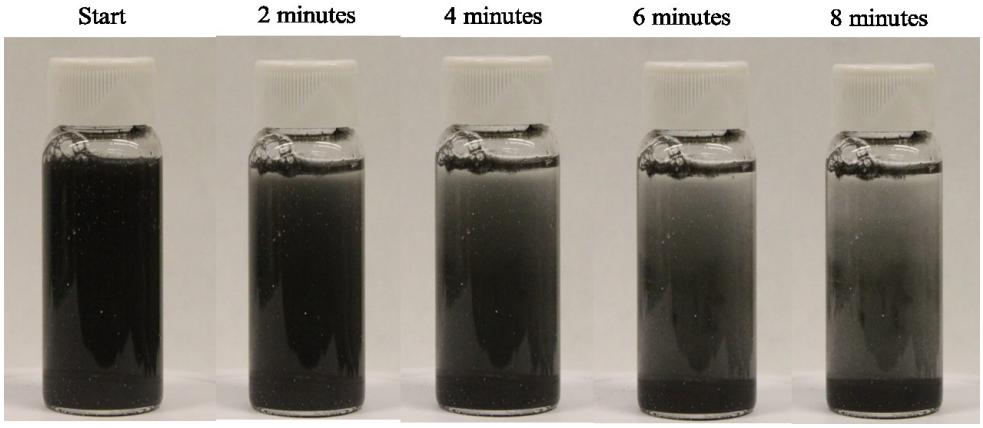

Figure 4.4 Images of the nickel nanoparticle suspension (prepared with 1.000 wt% CTAB surfactant) captured at different times after ultrasonication.

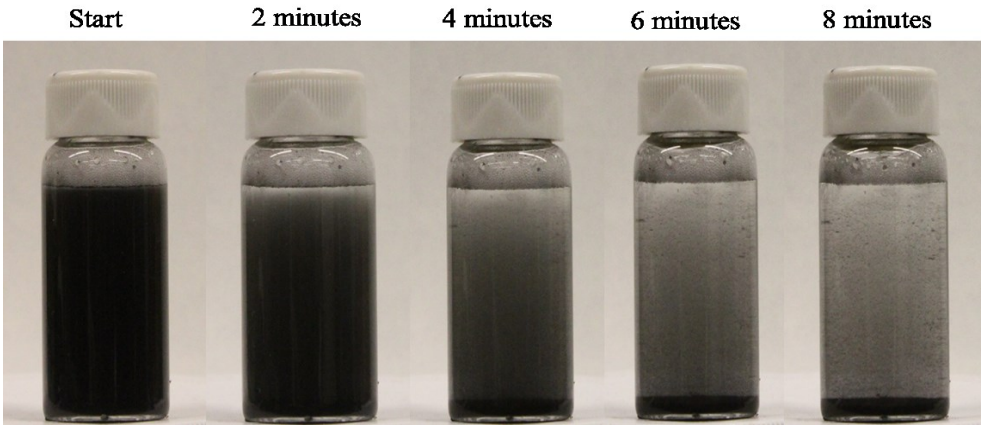

Figure 4.5 Images of the nickel nanoparticle suspension (prepared with 1.000 wt% CTAB and 0.030 wt% xanthan gum polymer) after ultrasonication.

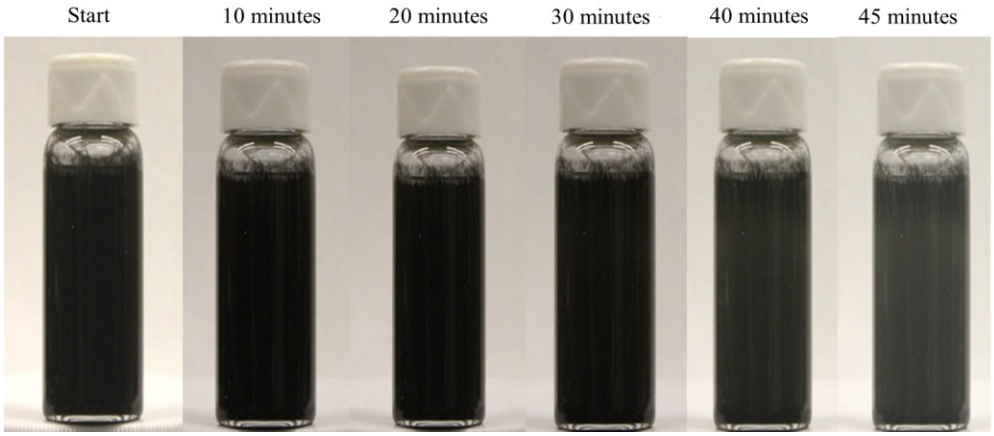

Figure 4.6 Images of the nickel nanoparticle suspension (prepared with 0.350 wt% SDS) after ultrasonication.

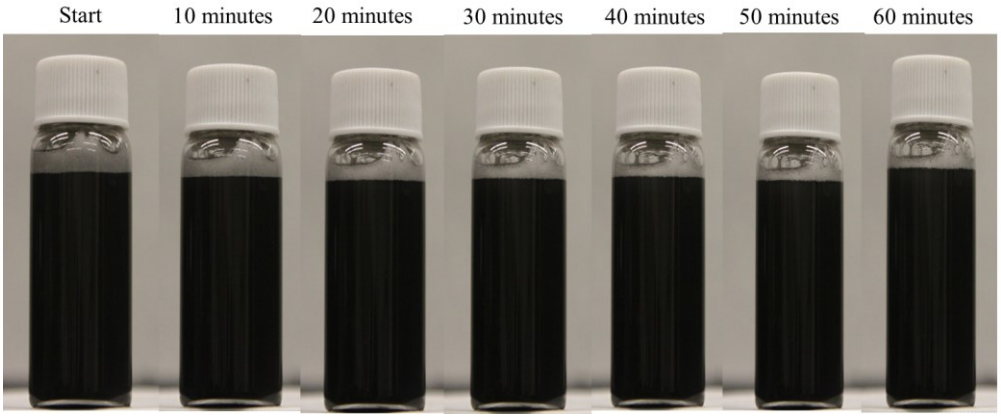

Figure 4.7 Images of the nickel nanoparticle suspension (prepared with 0.500 wt% SDS and 0.030 wt% xanthan polymer) captured at different times after ultrasonication.

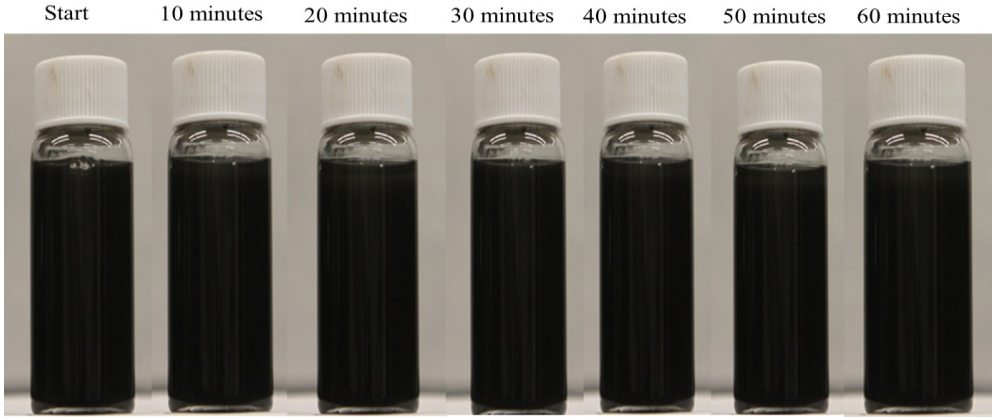

Figure 4.8 Images of the nickel nanoparticle suspension (prepared with 0.350 wt% Hypermer KD-2 and 0.045 wt% xanthan polymer) captured at different times after ultrasonication.

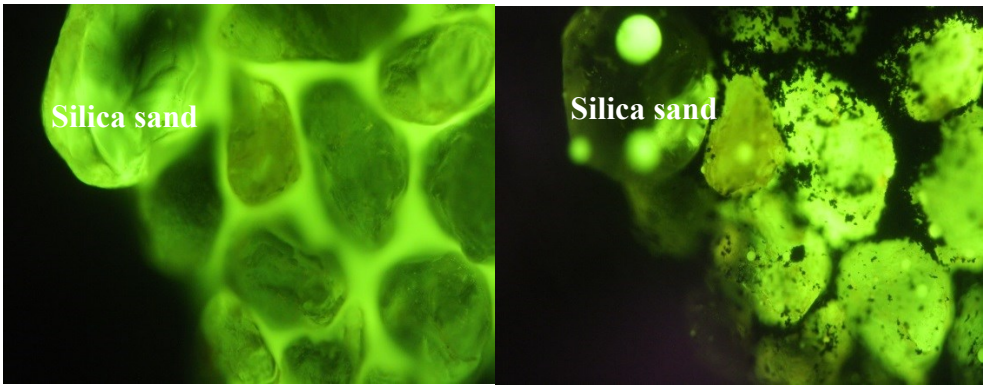

(a) **(b)**

Figure 4.9 The images near the injection port in the micromodel (a) before and (b) after the injection of 2.000 wt% nickel nanoparticle suspension prepared with 0.500 wt% SDS and 0.060 wt% xanthan gum polymer.

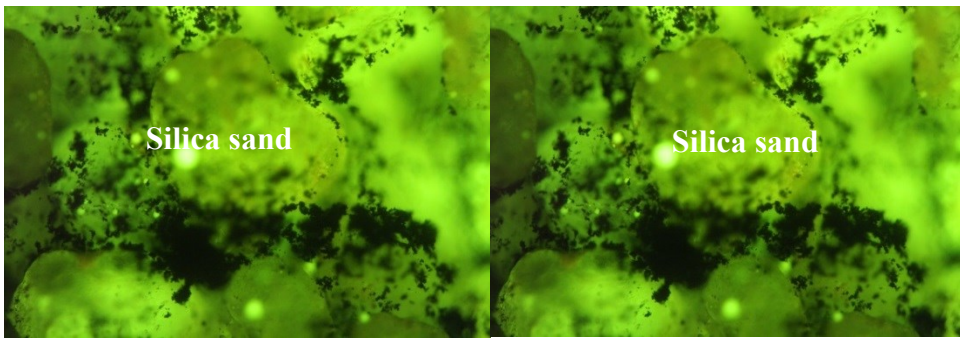

(a) **(b)**

Figure 4.10 Images taken at the same location in Exp #2.1 (a) before and (b) after water flooding.

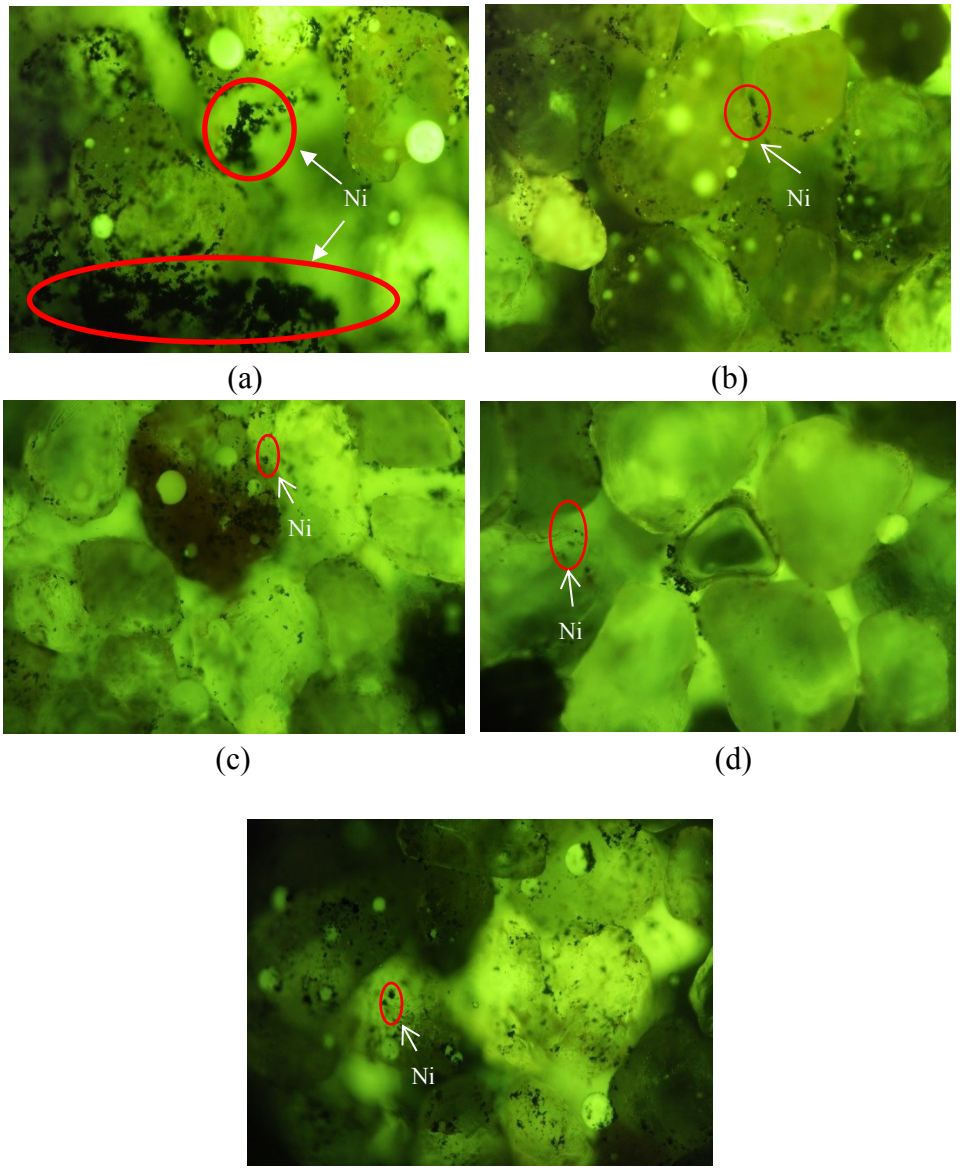

Figure 4.11 Images taken at different locations of the micromodel in Exp #2.1 after water flooding: (a) around injection port; (b) in the middle; (c) around the production end; (d) the upper part; and (e) the lower part.

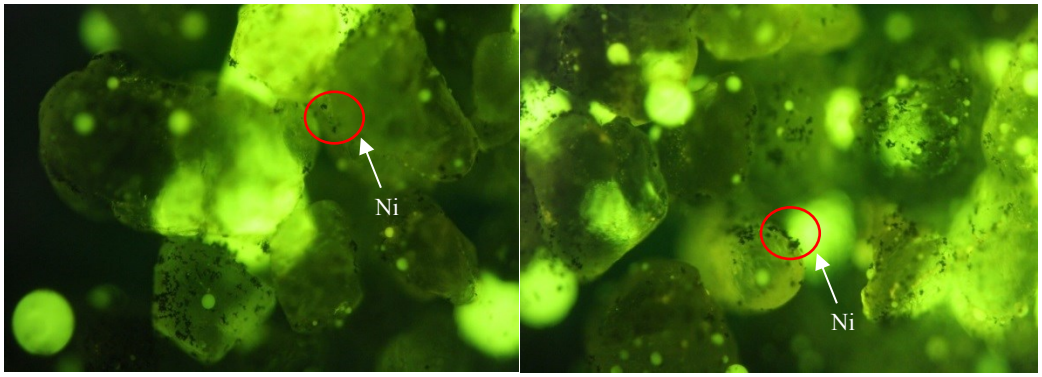

(a) (b)

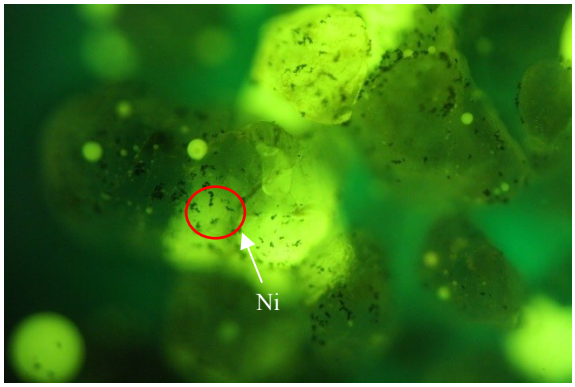

(c)

Figure 4.12 Images taken at different locations of the micromodel in Exp #2.2 after water flooding (1.000 wt% nickel nanoparticle suspension with SDS and xanthan gum polymer): (a) around injection port; (b) in the middle part; (c) near the production end.

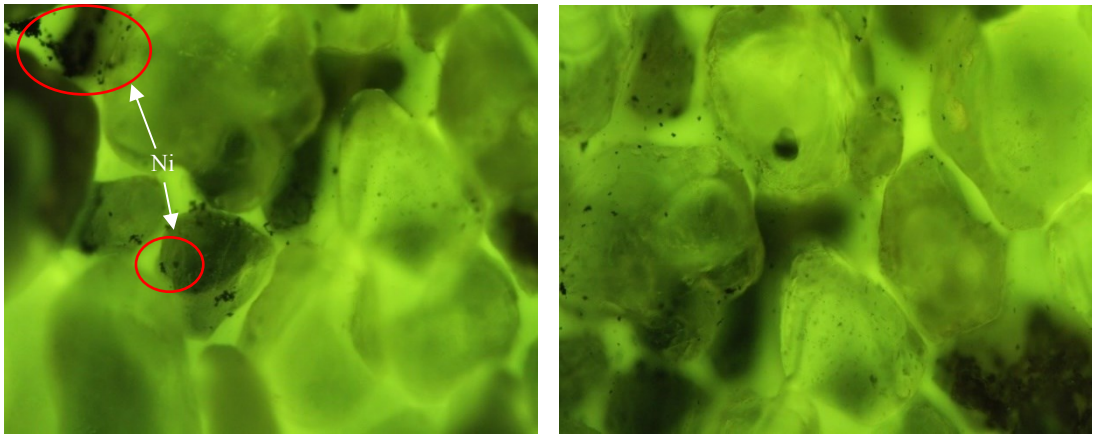

(a) (b)

Figure 4.13 Images taken at different locations of the micromodel in Exp #2.3 after water flooding (1.000 wt% nickel nanoparticle suspension with Hypermer KD-2 and xanthan gum polymer): (a) around the injection port; (b) around the production port.

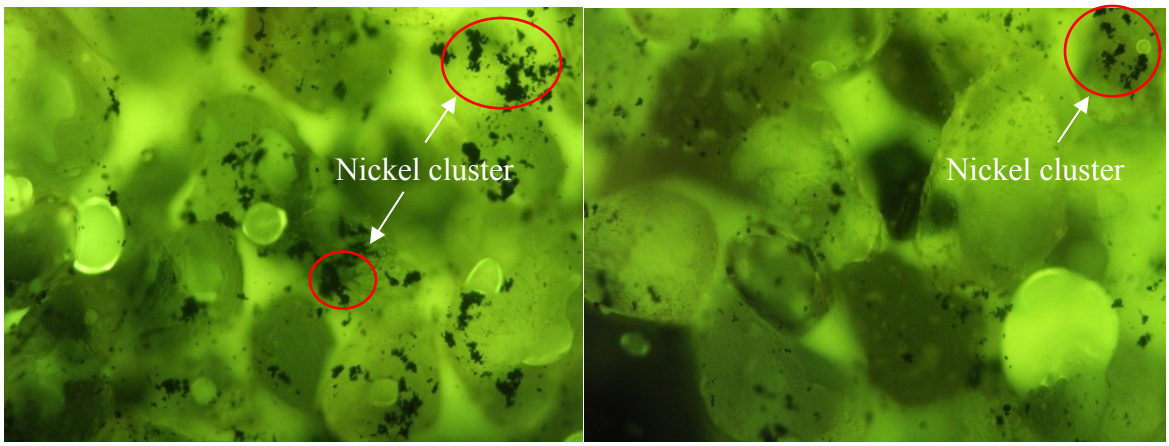

(a) **(b)**

Figure 4.14 Images taken at different locations of the micromodel in Exp #2.4 after water flooding (CTAB solution followed by 1.000 wt% nickel nanoparticle suspension with xanthan gum polymer): (a) injection port; (b) production port.

CHAPTER 5 Conclusions and Recommendations

5.1 Conclusions

This study conducted a series of CSS experiments to study the catalytic effect of nickel and iron oxide nanoparticle towards aquathermolysis reactions. These experiments were conducted by premixing the nanoparticles into the sand pack. To carry the nanoparticles into the deeper part of the reservoir, stable nanoparticle suspensions need to be created. We then conducted a detailed investigation on how to achieve stabilized nickel nanoparticle suspensions with the use of surfactant and polymer. Micromodel tests were conducted to examine how the nanoparticles were being migrating in the porous media when the nanoparticle suspension was being injected into the micromodel. The following conclusions can be obtained:

1. Both nickel and iron oxide nanoparticle can act as catalyst for aquathermolysis during CSS process and can break C-S bond effectively. However, the catalytic effect of nickel is stronger than iron oxide, thus a higher oil recovery and a lower oil viscosity can be obtained with the introduction of nickel nanoparticle. Moreover, in the experiments conducted with nickel nanoparticle, the catalytic effect tends to decrease with time, and even disappears in very late stages of CSS. This might be attributed to the decrease in the nickel concentration in the sandpack in later cycles;

2. The contribution of nickel nanoparticle for improving recovery factor mainly originated from the nanoparticles that were distributed near the injection port. The nickel nanoparticles should be placed deeper into the reservoir to achieve a better oil recovery in the long run. What's more, the use of nickel nanoparticles at 150°C had a certain upgrading effect at the very early stage of the CSS process; however, it could not improve the ultimate oil recovery in this study;

3. For the heavy oil sample used in this study, a nickel nanoparticle concentration of 0.05 wt% augmented the recovery most significantly in the early stages. A nickel nanoparticle concentration of 0.2 wt% applied at 220°C was found to be the optimum concentration yielding the highest overall recovery factor because the catalytic effect of nickel at a higher nickel nanoparticle concentration could last for a longer time;

4. After introducing nano-metal particles into the sand pack, the increase in oil recovery was also accompanied by a dramatic increase in the water production, especially in the early cycle. A higher amount of evolved gas, including hydrogen sulfide and alkenes was detected by GC analysis. Meanwhile, the recorded data shows that the pressure decline rate during soaking period for the experiments with metal nanoparticle was much slower than it in the base case. Thus, it is believed that the high gas production increased the reservoir pressure, hence leading to a higher water production;

5. In the later cycles of the CSS experiments, less fluid was present in the sandpack because more oil and water had been withdrawn from the sandpack in the earlier cycles of CSS tests with the use of nano-metal particles. This rendered the maintenance of the reservoir pressure more difficult. Because of this, the pressure decline could not be compensated by the gas production due to aquathermolysis reactions. This again explains why the amount of water produced in the later cycles of the experiments with the use of nano-metal particles was similar to that in the base case;

6. Each surfactant alone, i.e. CTAB, SDS, and Hypermer KD-2, could not well stabilize the nickel nanoparticle suspension at a concentration of 1 wt% or 2 wt%. Among these surfactants, cationic surfactant CTAB made the nickel nanoparticle settle in the shortest time. However, the stability of the nickel nanoparticle suspension could be significantly improved by introducing certain amount of Xanthan polymer into the system. The best recipes determined in this study are:

- 1 wt% Ni, 0.35 wt% SDS and 0.045 wt% Xanthan polymer;
- 1 wt% Ni, 0.35 wt% Hypermer KD-2 and 0.045 wt% Xanthan polymer; and
- 2 wt% Ni, 0.5 wt% Ni, and 0.06 wt% Xanthan polymer.

7. When a suspension containing a high nickel nanoparticle concentration was being injected into the porous media, the nickel nanoparticle tended to agglomerate severely and even block the channels near the injection port. However, this phenomenon disappeared at a lower nickel nanoparticle concentration; and

8. When nickel nanoparticle suspension was being injected into the porous media, only a small amount of the nickel nanoparticles could become attached to the surface of the sand

grains if the particle had the same surface charge with the silica sand. However, if the silica sands were first treated with CTAB surfactant to modify its surface charge from negative to positive, larger clusters around the sand grains could be formed and the particles became trapped.

5.2 Recommendations

To better simulate the field CSS conditions, the nano-metal particle should be injected into the reservoir in the form of nanoparticle suspension. Thus, additional experiments need to be conducted to investigate how the nano-metal particles, which are introduced into the sandpack through a suspension, will affect the recovery performance of CSS process. Further work is also needed to understand how the nanoparticles will transport in the sandpack as injection proceeds. The amount of nanoparticles produced along with oil and water should also be measured to quantify how much of the injected nanoparticles will be lost during the production period.

Whether the use of nano-metal particles in CSS is technically and economically feasible in a field scale is still in question unless it has been proved in field-scale pilot tests. It is thereby of critical importance to conduct pilot tests to confirm the many findings discovered in the laboratory experiments.

BIBLIOGRAPHY

Alaskar, M., Ames, M., Connor, S., et al. 2012. Nanoparticle and microparticle flow in porous and fractured media – An experimental study. 2012. *SPE J* **17** (04): 1-160.

Alvarez, J., and Han, S. 2013. Current overview of cyclic steam injection process. *J. Pet. Sci. Res.* **2** (3): 116-127.

Al-Marshed, A., Hart, A., Leeke, G., et al. 2015. Optimization of heavy oil upgrading using dispersed nanoparticulate iron oxide as a catalyst. *Energy Fuels*. **29** (10): 6306-16.

Bannerjee, D. 2012. Oil Sands, Heavy Oil and Bitumen: *From Recovery to Refinery*. 2012. Pennwell Corp.

Clark, P.D., Clarke, R.A., Hyne, J.B., et al. 1990a. Studies on the chemical reactions of heavy oils under steam stimulation conditions. *AOSTRA J. Res.* **6** (1): 29-39.

Clark, P.D., Clarke, R.A., Hyne, J.B., et al. 1990b. Studies on the effect of metal species on oil sands undergoing steam treatments. *AOSTRA J. Res.* **6** (1): 53-64.

Clark, P.D., and Hyne, J.B. 1983. Steam-oil chemical reactions: mechanisms for the aquathermolysis of heavy oils. *AOSTRA J. Res.* **1** (1): 15-20.

Eakin, B.E., Mitch, F.J., and Hanzlik, E.J. 1990. Oil property and composition changes caused by water injection. Paper SPE-20738 presented at the 65th SPE Annual Technical Conference and Exhibition, New Orleans, Louisiana, 23-26 September.

Fan, H, Liu, Y., Zhang, L. et al. 2002. The study on composition changes of heavy oils during steam stimulation process. *Fuel* **81**: 1733-1738.

Fan, H., Zhang, Y., and Lin, Y. 2004. The catalytic effects of minerals on aquathermolysis of heavy oils. *Fuel* **83**: 2035-2039.

Farouq Ali, S.M. 1994. CSS – Canada's super strategy for oil sands. *J. Can. Petro. Tech.* **33** (9):16-19.

Farooqui, J., Babadagli, T., and Li, H. 2015. Improvement of the recovery factor using nano-metal particles at the late stages of cyclic steam stimulation. Paper SPE-174478-MS presented at the SPE Canada Heavy Oil Technical Conference, Calgary, Alberta, Canada, 9-11 June.

Franco, C.A., Cardona, L., Lopera, S.H., et al. 2016. Heavy oil upgrading and enhanced recovery in a continuous steam injection process assisted by nanoparticulated catalysts. Paper SPE-

179699-MS presented at SPE Improved Oil Recovery Conference, Tulsa, Oklahoma, USA, 11-13 April.

Gu, H., Cheng, L., Huang, S., et al. 2015. Steam injection for heavy oil recovery: Modelling of wellbore heat efficiency and analysis of steam injection performance. *Energ. Convers. Manage.* **97**: 166-177.

Hamedi-Shokrlu, Y. and Babadagli, T. 2013. In-Situ upgrading of heavy oil/bitumen during steam injection by use of metal nanoparticles: A study on in-situ catalysis and catalyst transportation. Paper SPE-146661 presented at the SPE Annual Technical Conference and Exhibition, Denver, Colorado, 30 October -2 November.

Hamedi-Shokrlu, Y. and Babadagli, T. 2014a. Viscosity reduction of heavy oil/bitumen using micro- and nano-metal particles during aqueous and non-aqueous thermal applications. *J. Petro. Sci. Eng.* **119**: 210-220.

Hamedi-Shokrlu, Y. and Babadagli, T. 2014b. Kinetics of the in-situ upgrading of heavy oil by nickel nanoparticle catalysts and its effect on cyclic-steam-stimulation recovery factor. *SPE. Res. Eval. Eng.* **17** (3): 355-364.

Hashemi, R., Nassar, N.N., and Pereira Almao, P. 2013. Enhanced heavy oil recovery by in situ prepared ultradispersed multimetallic nanoparticles: A study of hot fluid flooding for Athabasca bitumen recovery. *Energ Fuel*. **27** (4): 2194-2201.

Hwang, Y., Lee, J.K., Lee, J.K., et al. 2008. Production and dispersion stability of nanoparticles in nanofluids. *Powder Thchnol. 186*(2):145-153.

Hyne, J.B. 1986. Aquathermolysis - A synopsis of work on the chemical reactions between water (steam) and heavy oil sands during simulated steam stimulation. Synopsis report No.50, AOSTRA contracts No. 11, 103, 103B/C.

Kim, C.K., Lee, G.J., Lee, M.K., et al. 2015. A study on dispersion stability of nickel nanoparticles synthesized by wire explosion in liquid media. *Arch. Metall. Mater*. **60** (2): 1379-1382.

Kong, X. and Ohadi, M. 2010. Applications of micro and nano technologies in the oil and gas industry-overview of the recent progress. Paper SPE-138241-MS Presented at SPE International Petroleum Exhibition and Conference, Abu Dhabi, Dubai, 1-4 November.

Li, X., Zhu, D., and Wang, X. 2007. Evaluation on dispersion behavior of the aqueous copper nano-suspensions. *J Colloid Interf Sci*. **310** (2): 456-463.

Mollaei, A., Maini, B. 2010. Steam flooding of naturally fractured reservoirs: basic concepts and recovery mechanisms. *J. Can. Petro. Tech.* **49** (1): 65-70.

Moon, Y.K., Lee, J.K., Kim, J.G., et al. 2009. Sintering kinetic measurement of nickel nanoparticle agglomerates by electrical mobility classification. *Current Applied Physics* **9** (5): 928-932.

Pierre, C., Barre, L., Pina, A., and Moan, M. 2004. Composition and heavy oil rheology. *Oil Gas Sci. Tech*. **59** (5): 489-501.

Sheng, J.J. 2013. *Enhanced oil recovery field case studies*. Gulf Professional Publishing.

Tjoeng, A.Y. and Loro, R. 2016. Viscosity modelling of Pyrenees crude oil emulsions. Paper SPE 182326 presented in the Asia Pacific Oil & Gas Conference and Exhibition, Perth, Australia. 25-27 October.

Rahimi, P.M. and Gentzis, T. 2006. The chemistry of bitumen and heavy oil processing. In *Practical advances in petroleum processing,* eds. C.S. Hsu and P.R. Robinson, Chap. 19, 149-179. New York City, New York: Springer New York.

Ragab, A.M.S. and Hannora, A.E. 2015. An experimental investigation of silica nano particles for enhanced oil recovery applications. SPE-175829-MS Presented at SPE North Africa Technical Conference and Exhibition, Cairo, Egypt, 14-16 September.

Wei, L., Zhu, J.H., and Qi, J.H. 2007. Application of nano-nickel catalyst in the viscosity reduction of Liaohe extra-heavy oil by aqua-thermolysis. *J. Fuel Chem. Technol*. **35** (2): 176-180.

Williams, W.C., Bang, I.C., Forrest, E., et al. 2006. Preparation and characterization of various nanofluids. In: *Proceedings of the NSTI Nanotechnology Conference and Trade Show (NANOTECH 06).* (2): 408-411.

Wu, Y., Carroll, J. 2011. Acid gas injection and related technologies. John Wiley & Sons.

Xue, D. and Sethi, R. 2012. Viscoelastic gels of guar and xanthan gum mixtures provide long-term stabilization of iron micro-and nanoparticles. *J. Nanopart. Res*. **14** (11): 1239.

Yi, S., Babadagli, T., and Li, H.A. 2017. Use of nickel nanoparticles for promoting aquathermolysis reaction during cyclic steam stimulation. *SPE J.* In press.